

## The SOL (*Solar Origin and Life*) Project: Detailed characterization of candidates for the ZAMS and Subgiant stages

EDUARDO-OLIVEIRA C.S. ,<sup>1</sup> GHEZZI, L. ,<sup>1,2</sup> PORTO DE MELLO, G. F. ,<sup>1</sup> LORENZO-OLIVEIRA, D. ,<sup>3</sup>  
 SOUZA DOS SANTOS, P. V. ,<sup>1</sup> AND COSTA-ALMEIDA, E. <sup>2</sup>

<sup>1</sup>Observatório do Valongo, Universidade Federal do Rio de Janeiro, Ladeira do Pedro Antonio, 43, 20080-090 Rio de Janeiro, Brazil

<sup>2</sup>Observatório Nacional, MCTIC (ON), Rua Gal. José Cristino 77, São Cristóvão, 20921-400, Rio de Janeiro, Brazil

<sup>3</sup>Laboratório Nacional de Astrofísica, Rua Estados Unidos 154, 37504-364, Itajubá - MG, Brazil

### ABSTRACT

The context of the Sun in the galactic neighborhood is not well understood, especially when we compare its physical properties to those of nearby stars. Thereby, we still cannot fully comprehend whether or not the Sun is a typical star. This work aims to identify and characterize stars aligned with the solar evolutionary track that could represent it at the ZAMS and subgiant stages. We performed a spectroscopic analysis of 18 photometrically selected candidates using high-resolution and high-SNR spectra as well as the classical spectroscopic method, based on the excitation and ionization equilibria of Fe I and Fe II lines. Additionally, we derived evolutionary parameters using isochrones, and kinematic parameters. We also estimated chromospheric activity levels and performed age estimates through 3 additional independent methods: activity-age relations using the Ca II H & K and H $\alpha$  lines, and rotation periods estimated from TESS light curves. We identified three candidates that provide a good match to the Sun at  $\approx 0.5$  Gyr (HD 13531 and HD 61033) and subgiant (HD 148577) stages. Moreover, HD 197210 could be of interest when studying the Sun at  $\approx 2$  Gyr, when the Earth's atmosphere started having a significant amount of oxygen. Our selection method was successful and we were able to identify stars similar to the Sun at different evolutionary stages, which is essential for future research in the search of exoplanets and understand habitability, especially with the advent of the next generation of exoplanet-hunting instruments.

**Keywords:** Solar analogs (1941) — Fundamental parameters of stars (555) — Solar evolution (1492)  
 — Solar neighborhood (1509)

### 1. INTRODUCTION

The Sun is currently the only star known to harbor a planet onto which life flourished. This striking feature could be a direct result of many possible peculiarities it exhibits when compared to stars in the solar neighborhood. The Sun's location possibly minimizes the number of passages through the spiral arms, decreasing the probabilities of exposure to close-by supernova events or encounters with giant molecular clouds that could disturb the Solar System. Therefore, the Sun's location in the Galaxy might have been fundamental to the long-term maintenance of a suitable biosphere for life on Earth as well as to limit the amount of mass extinction events (E. M. Leitch & G. Vasisht 1998; G. Porto de Mello et al. 2006; G. F. Porto de Mello et al. 2009). However, its birthplace could be located at a Galactocentric radius  $R_g \approx 5 - 6$  kpc followed by an outward migration to its current position (M.-F. Nieva & N. Przybilla 2012) close to galactic corotation (J. Lépine et al. 2001).

Furthermore, there was early evidence that the Sun is metal-rich for its age (H. J. Rocha-Pinto & W. J. Maciel 1996). However, L. Casagrande et al. (2011) presented a new revision of the Geneva-Copenhagen survey and their results suggest that the Sun is indeed a typical star when we compare its metallicity to the distribution of metallicities of the solar neighborhood. Other possible chemical peculiarities have been suggested for the Sun, such as a higher C/O ratio relative to the cosmic abundance standard (CAS) (M.-F. Nieva & N. Przybilla (2012), but see also M.

Asplund et al. 2009), a larger Li depletion relative to solar-type stars (e.g., L. Pasquini et al. 1994; Y. Takeda et al. 2007; I. Ramírez et al. 2012; M. Carlos et al. 2025; but see also L. Ghezzi et al. 2010) and deficiency in refractory elements relative to volatiles when compared to the so-called solar twin stars (e.g., J. Meléndez et al. 2009; R. A. Booth & J. E. Owen 2020; R. Rampalli et al. 2024). The first feature influences the structure of the planets that will be formed in the system, while the second and the third could be a consequence of giant or terrestrial planet formation, respectively. However, the effect of depletion of refractory elements could also be reproduced through a combination of multiple factors that may have acted simultaneously (such as the chemical evolution of the Galaxy, the Sun's possible migration, and processes intrinsic to the protoplanetary disk), making it very difficult to independently quantify their individual contributions (B. Gustafsson 2025).

There is also some evidence that the Sun might have a longer rotational period (G. Pace & L. Pasquini 2004; but see also L. A. Dos Santos et al. 2016) and a lower chromospheric activity level (J. C. Hall & G. Lockwood 2000) than stars of similar age, both of which are possibly connected with the enhanced Li depletion. However, recent studies suggest that the Sun is not an uncommon star, considering its age and spectral type (J. C. Hall et al. 2007; T. Reinhold et al. 2020). Nonetheless, its activity cycles seem smoother and more regular when compared to Sun-like stars (R. R. Radick et al. 2018). This factor could have played a significant role in the habitability of our Solar System.

More recently, G. Gonzalez (2025) performed a comprehensive statistical analysis to search for anomalous properties that the Sun may exhibit within a large sample of nearby stars (up to 25 pc), including solar analogs and twins. He identified its mass (top  $\approx$ 8 per cent), low photometric variability on short timescales (bottom  $\approx$ 0.2 per cent), specific light and heavy element abundance patterns, slow rotation, and low superflare rate as its most peculiar characteristics.

It is thus clear that an investigation of the solar properties relative to similar stars and a detailed description of its evolution are extremely important for understanding how life appeared and evolved on Earth as well as for the searches for habitable planets and extraterrestrial life. For this reason, our group has been analyzing stars that follow the solar evolutionary track on the HR diagram to search for proxies that could represent the Sun at different stages of its evolution. The first results of this effort were the identification of the solar twin 18 Sco (HD 146233, HR 6060; G. Porto de Mello & L. da Silva 1997), which persists as one of the best candidates found to date. More recently, we identified 10 new likely solar twins that are being subjected to more detailed analyzes (G. Porto de Mello et al. 2014). These stars add up to a much larger sample of candidates to solar analogs and twins that were proposed by different groups over the past decades (e.g., J. Hardorp 1978; G. Cayrel de Strobel et al. 1981; G. Cayrel de Strobel 1996; C. Soubiran & A. Triaud 2004; J. R. King et al. 2005; Y. Takeda et al. 2007; J. Meléndez et al. 2009; A. Önehag et al. 2011; I. Ramírez et al. 2014; J. Yana Galarza et al. 2021; C. Lehmann et al. 2022).

Since stars that resemble the current Sun do not provide the entire picture about its evolution, the searches described above were extended to other evolutionary stages along a solar evolutionary track. I. Ribas et al. (2010) presented a detailed analysis of  $\kappa^1$  Cet, which is an analog of the Sun when life appeared on Earth. J.-D. Do Nascimento et al. (2013) analyzed CoRoT ID 102684698, which is an evolved solar twin that could provide insights into the future of the Sun. Solar proxies in different evolutionary stages were also found by the Sun in Time program (e.g., J. D. Dorren & E. F. Guinan 1994; M. Güdel et al. 1997; I. Ribas et al. 2005, 2010) as well as by other groups (D. Dravins et al. 1993c,b,a; E. J. Gaidos 1998; J. Y. Galarza et al. 2025).

In order to continue and extend previous initiatives, we started the *Solar Origin and Life* (SOL) project back in 2003. The main goal of this effort is to identify stars that resemble the Sun along its evolutionary path in order to understand how its properties influenced the formation and evolution of the Solar System and life on Earth. In this paper, we present the pilot study for this project and the resulting candidates we identified. Section 2 describes the sample selection, observations and data reduction. Section 3 contains the determination of the atmospheric, evolutionary and kinematical parameters, as well as the activity indicators in Section 4. In Section 5, we discuss the results and use them to carefully select the best candidates to represent the Sun. Our concluding remarks are presented in Section 6.

## 2. SAMPLE SELECTION AND DATA

### 2.1. Sample Selection

Any study that attempts to select solar proxies which lie along or close to its evolutionary path will be naturally model dependent. We decided to adopt as our reference the evolutionary track from G. Schaller et al. (1992) that was calculated for  $1 M_{\odot}$  and  $Z = 0.02$ . These models do not take overshooting and rotation into account and had to be adjusted so that a point with an age of 4.56 Gyr (adopted from J. N. Connelly et al. 2012) corresponded to the current solar effective temperature ( $T_{eff} \approx 5780$  K) and luminosity. Although more recent evolutionary tracks are available

in the literature, we opted for this grid because its uses a similar physics as the one employed by I. Sackmann et al. (1993) and we wanted to benefit from the wealth of information contained in this latter study. Moreover, we wanted to keep this pilot study consistent with previous selections performed by our group (e.g., G. Porto de Mello et al. 2014). We note, however, that comparisons with similar but more recent evolutionary tracks (e.g., P. Demarque et al. 2004; Y. Chen et al. 2015) did not reveal discrepancies that would significantly affect our results for the evolutionary stages analyzed here. We chose the evolutionary tracks of G. Schaller et al. (1992) to maintain consistency with G. Porto de Mello et al. (2014). We note that more recent evolutionary tracks are available such as PARSEC (A. Bressan et al. 2012) and Dartmouth (A. Dotter et al. 2008); however, the differences in  $T_{\text{eff}}$  ( $\Delta_{\text{max}} = 70K$ ) are below the typical external uncertainties found in the comparisons of parameters for solar-type stars (e.g., N. R. Hinkel et al. 2016) and the differences in luminosity ( $\Delta_{\text{max}} = 0.03$ ) are consistent with our internal uncertainties (mean  $\sigma_{L/L_{\odot}} = 0.02$  for the ZAMS and mean  $\sigma_{L/L_{\odot}} = 0.05$  for the SG candidates), as will be shown in Sections 3.1 and 3.3.

Following the detailed discussion performed in Section 3.2 of I. Sackmann et al. (1993), we chose two stages, Zero Age Main Sequence (ZAMS) and Subgiant (SG), along our reference solar evolutionary track that are related to the points in their Figure 2. Their corresponding effective temperatures and luminosities are given in Table 1, in which we also show the parameters of the Present Sun (as given by G. Schaller et al. 1992) for comparison. The stage in which the Sun enters on the main sequence is represented by the point ZAMS (Zero Age Main Sequence) and it was chosen according to point A in Figure 2 of I. Sackmann et al. (1993). We can see that it is cooler, less luminous and smaller than the current Sun, shown by the point Today. The stage in which the Sun leaves the main sequence is depicted by the point TO (turn-off). At this moment, the Sun will be slightly cooler, but  $\approx 34\%$  larger and  $\approx 76\%$  more luminous.

The selection of stars that could represent the Sun in these two evolutionary stages (ZAMS and SG) was performed by L. Ghezzi (2005) and relies on the photometric boxes in the  $M_{V_T}$  -  $(B_T - V_T)$  plane, as described by G. Porto de Mello et al. (2014). Briefly, we converted the luminosities in Table 1 to absolute visual magnitudes  $M_{V_T}$  in the  $V_{Tycho}$  band using  $M_{bol_{\odot}} = 4.81$  (as adopted in G. Porto de Mello et al. 2014) and bolometric corrections from G. Habets & J. Heintze (1981). The color indexes ( $B_T - V_T$ ) were calculated using the photometric calibration from L. Ghezzi (2005), which was determined following a similar procedure as the one described in the Appendix A of G. Porto de Mello et al. (2014). The inputs to the calibration are the effective temperatures, taken from Table 1, and the solar metallicity, which was set to  $[\text{Fe}/\text{H}] = 0.00$  by definition. The values for  $M_{V_T}$  and  $(B_T - V_T)$  for the Sun ZAMS and SG are shown in Table 1.

In order to set the widths of the photometric boxes around these points, we need their uncertainties. These were estimated in the same way as described by G. Porto de Mello et al. (2014). As we decided to perform the cut  $V_T < 8.1$  in order to select only the brightest stars for our pilot study, the values of these uncertainties are  $\sigma(M_{V_T}) = 0.07$  and  $\sigma(B_T - V_T) = 0.013$  (G. Porto de Mello et al. 2014). We constructed our photometric boxes considering  $2\sigma$  intervals around the photometric points for the Sun ZAMS and SG. Finally, we searched the Hipparcos catalog (M. A. Perryman et al. 1997) for stars within these photometric boxes that also had  $V_T < 8.1$ ; since our selection was carried out before the launch of Gaia ( Gaia Collaboration et al. 2018), we decided to use Hipparcos; future selections of our project will make use of Gaia data.

We selected 20 candidates but removed two stars from our sample. One of them (HD 114260) is a spectroscopic binary<sup>4</sup> and the determination of spectroscopic parameters might be affected by the contamination of the spectral lines from the secondary. For the other one (HD 215028), we were not able to observe or retrieve from public archives a spectrum with the minimum quality required (see Section 2.2) for our detailed analysis. Our final sample contains 18 stars, 8 of which are candidates to the ZAMS stage and 10 to the SG stage. Furthermore, we decided to include the solar twin 18 Sco (HD 146233) as a control star in the sample, as it is well studied in the literature (e. g., G. Porto de Mello & L. da Silva 1997, M. Bazot et al. 2011, I. Ramírez et al. 2014, M. Bazot et al. 2018, J.-D. Do Nascimento et al. 2023), and we can use it to check the precision of our method.

## 2.2. Data and reduction

The data for our sample stars were obtained from two main sources. The spectra of 2 stars were obtained using the MUSICOS *echelle* spectrograph attached to the 1.6m telescope at Pico dos Dias Observatory (OPD) between 2013 and 2017. The Pico dos Dias Observatory and MUSICOS are administered by Laboratório Nacional de Astrofísica (LNA) and its resolving power is approximately  $R \approx 35000$  with a spectral coverage of 5400-8800Å. We reduced the

<sup>4</sup> <https://simbad.u-strasbg.fr/simbad/sim-basic?Ident=HD+114260>

MUSICOS spectra using standard procedures (bias, flat-field and scattered light corrections; one dimensional extraction and wavelength calibration).

The other main source was public databases from the following spectrographs: FEROS/ESO (A. Kaufer et al. 1997), UVES/ESO (H. Dekker et al. 2000), HARPS-S/ESO (M. Mayor et al. 2003), HARPS-N/TNG (R. Cosentino et al. 2012), HIRES/KECK (S. S. Vogt et al. 1994) and ESPaDOnS/CFHT (J.-F. Donati 2003). In addition to the MUSICOS's spectra, we were able to retrieve high-quality spectra for our candidates with resolving powers ranging from 35000 up to 115000 and minimum signal-to-noise ratio (SNR) of 100. We acquired almost 90 high-quality spectra for our 18 candidates and 18 Sco, which resulted in a better estimation of the fundamental parameters of the candidates. The public spectra were already reduced by their own automated pipelines.

We corrected all spectra for their Doppler shifts using the *fxcor* and *dopcor* tasks from IRAF (Image Reduction and Analysis Facility)<sup>5</sup> and a solar rest-frame spectrum as reference (K. Hinkle et al. 2000). Finally, we estimated their SNR values using IRAF's *bplot* routine on 143 continuum regions carefully selected using the solar flux spectrum from K. Hinkle et al. (2000). After performing 2 rounds of  $2\sigma$  clipping we established their mean value as the final one for each spectra (see Table 2). We note that although our spectroscopic data are not homogeneous, this did not affect the internal consistency of our results (see Section 3.1).

**Table 1.** Values adopted from I. Sackmann et al. (1993) for the evolutionary stages discussed in this work. The canonical values of the present Sun were included for comparison purposes.

Stage	$T_{eff}$ (K)	L ( $L_{\odot}$ )	R ( $R_{\odot}$ )	Age (Gyr)	( $M_{V_T}$ )	( $B_T-V_T$ )
ZAMS	5586	0.70	0.897	0.0	5.36	0.81
Present Sun	5777	1.00	1.000	4.5	4.88	0.73
SG	5743	1.76	1.343	10.0	4.30	0.75

<sup>5</sup> <https://iraf-community.github.io/>

**Table 2.** All input parameters of the sample stars that were used throughout the analysis. The columns in the table represent: ID, spectral type, the evolutionary stage for which the candidate was selected, parallax, magnitude in the V band, RA and DEC coordinates, proper motion in RA and DEC, radial velocity, number of spectra analyzed, source instruments and the SNR interval.

Star	Spectral type	Candidate	$\pi$ (mas)	V (mag)	RA (degrees)	Dec (degrees)	$\mu_\alpha$ (mas/yr)	$\mu_\delta$ (mas/yr)	$V_{rad}$ $km\,s^{-1}$	$N_{spectra}$	Instrument(s)
HD 13531	G7V	ZAMS	38.27 $\pm$ 0.06	7.36 $\pm$ 0.01	33.31	40.51	59.262	-90.533	6.70	3	ESPaDOnS
HD 21411	G8V	ZAMS	34.30 $\pm$ 0.04	7.88 $\pm$ 0.01	51.55	-30.62	218.073	226.095	17.80	3	HARPS-S
HD 25918	G5	ZAMS	30.76 $\pm$ 0.06	7.72 $\pm$ 0.01	62.06	44.66	-298.823	-133.236	-36.15	3	SOPHIE
HD 55720	G8V	ZAMS	36.21 $\pm$ 0.03	7.47 $\pm$ 0.01	107.88	-49.42	-7.129	817.422	87.41	1	FEROS
HD 61033	G7V	ZAMS	36.06 $\pm$ 0.96	7.57 $\pm$ 0.01	113.62	-52.97	-25.532	271.951	14.98	1	FEROS
HD 64114	G7V	ZAMS	31.69 $\pm$ 0.04	7.72 $\pm$ 0.01	117.98	-11.03	-69.453	-173.481	53.18	1	FEROS
HD 182619	G5	ZAMS	30.53 $\pm$ 0.04	7.80 $\pm$ 0.01	291.17	22.20	134.856	-83.177	8.27	3	SOPHIE
HD 197210	G5V	ZAMS	33.50 $\pm$ 0.04	7.61 $\pm$ 0.01	310.62	-5.30	-60.414	-172.389	3.22	6	HARPS-N, HARPS-S
HD 15942	G0	SG	22.39 $\pm$ 0.04	7.50 $\pm$ 0.01	38.52	12.18	183.713	-35.560	34.24	3	HARPS-S
HD 19308	G0	SG	25.70 $\pm$ 0.07	7.37 $\pm$ 0.01	46.91	36.62	241.022	-217.657	32.74	3	SOPHIE
HD 24040	G1	SG	21.42 $\pm$ 0.06	7.50 $\pm$ 0.01	57.60	17.48	113.215	-251.033	-9.34	6	SOPHIE, UVES
HD 69809	G0	SG	18.75 $\pm$ 0.05	7.86 $\pm$ 0.01	124.81	14.20	35.895	24.442	17.47	5	Hires, UVES
HD 74698	G5V	SG	19.18 $\pm$ 0.03	7.76 $\pm$ 0.01	130.07	-71.88	106.122	61.270	38.75	3	HARPS-S
HD 111398	G5V	SG	27.50 $\pm$ 0.05	7.10 $\pm$ 0.01	192.22	12.10	233.049	-139.621	3.18	3	SOPHIE
HD 148577	G5V	SG	18.52 $\pm$ 0.05	7.96 $\pm$ 0.01	247.43	-18.68	81.435	-238.526	62.74	4	HARPS-S, MUSICOS
HD 175425	G0	SG	18.56 $\pm$ 0.03	7.89 $\pm$ 0.01	283.41	37.99	-46.687	-84.223	-67.74	1	Hires
HD 196050	G3V	SG	19.71 $\pm$ 0.04	7.49 $\pm$ 0.01	309.47	-60.63	-191.122	-64.922	61.37	7	FEROS, HARPS-S, UVES
HD 213575	G5V	SG	26.73 $\pm$ 0.09	6.95 $\pm$ 0.01	338.14	-6.47	291.969	30.281	-21.50	12	SOPHIE, UVES
18 Sco	G2V	TWIN	70.77 $\pm$ 0.11	5.50 $\pm$ 0.01	243.91	-8.37	232.159	-495.368	11.76	20	ESPaDOnS, FEROS, HARPS-N, HARPS-S, HIRES, SOPHIE, UVES, MUSICOS

### 3. STELLAR PARAMETERS

#### 3.1. *Atmospheric parameters*

We determined the atmospheric parameters of the stars in our sample using the classical spectroscopic method based on the excitation and ionization equilibria of Fe I and Fe II lines. We used ARESV2 (S. Sousa et al. 2007; S. Sousa et al. 2015) to automatically measure the equivalent widths of 176 lines from the list of L. Ghezzi et al. (2018). We adopted the following input parameters for ARESV2: *smoothder* = 4, *space* = 3.0, *lineresol* = 0.1, and *miniline* = 5. The *rejt* parameter was set to the measured SNR of the spectra as described in the Section 2.2.

We determined the atmospheric parameters ( $T_{eff}$ ,  $\log g$ , [Fe/H],  $\xi$ ) of the 18 candidates in our sample using the same pipeline as L. Ghezzi et al. (2018, 2021). The analysis was done in LTE using the 2017 version of MOOG<sup>6</sup> (C. A. Sneden 1973) along with the ATLAS9 ODFNEW grid (F. Castelli & R. L. Kurucz 2003) to generate interpolated model atmospheres. The final parameters for each star are obtained through a non-differential iterative process that has to simultaneously meet four criteria based on the excitation and ionization equilibria of Fe I and Fe II spectral lines. These criteria are: no correlation between A(Fe I) and the excitation potential  $\chi$  (excitation equilibrium) and between A(Fe I) and the reduced equivalent width  $\log(EW/\lambda)$ ; same average values of A(Fe I) and A(Fe II) (ionization equilibrium); and same value for the metallicity in the input model atmosphere and the output result from MOOG. This process is repeated by changing the input values of  $T_{eff}$ ,  $\xi$ ,  $\log g$ , [Fe/H], respectively, until convergence of the four criteria is achieved. The last step of the automated process is to perform a round of  $2\sigma$  clipping to remove outliers, i.e., lines with corresponding abundances that present large deviations from the average, after that, the entire iteration process is repeated. An example of the final convergence can be seen in the Figure 1 for the ZAMS candidate HD 13531. The uncertainties of the atmospheric parameters were estimated following the procedures of L. Ghezzi et al. (2018, 2021).

<sup>6</sup> <https://www.as.utexas.edu/~chris/moog.html>

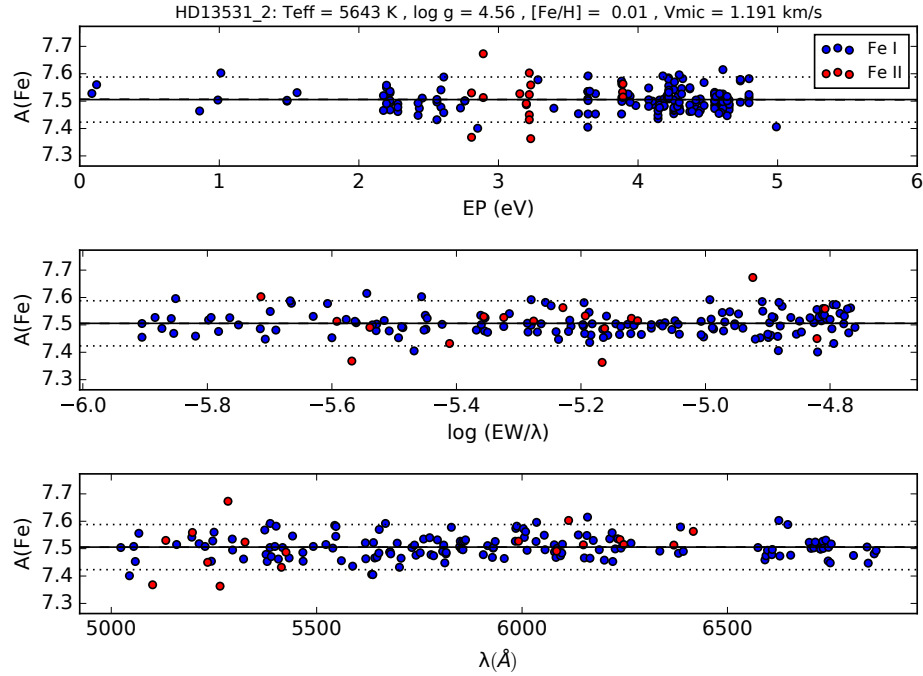


**Figure 1.** Final result of the atmospheric parameters iteration for the ZAMS candidate HD 13531, using the EW measurements from a ESPaDOnS spectrum (SNR = 310). Upper panel: No trend between the determined  $A(\text{Fe I})$  abundances and the excitation potential. Middle panel: No trend between the  $A(\text{Fe I})$  abundances and the reduced equivalent width  $\log(\text{EW}/\lambda)$  of each line. Lower panel: determined abundances as a function of the wavelength of each spectral line. The blue dots represent the Fe I abundances, while the red dots represent the Fe II abundances. The solid lines show the mean  $A(\text{Fe})$  abundance. The dashed lines (which overlaps with the solid line because convergence was achieved) show the linear fits performed. The dotted lines show  $2\sigma$  limits around the mean.

The derived atmospheric parameters from each spectrum of our sample stars are shown in the Figure 2, where the black stars represent the expected atmospheric parameters of the Sun during the respective evolutionary stage. The final atmospheric parameters and their associated uncertainties can be seen in Table 3. As mentioned before, this analysis was performed for all spectra of our candidate stars. The internal agreement between each observation of the candidates is excellent and their estimated parameters values agree with the mean value within a  $2\sigma$  interval for every candidate.

In the end of the process, we took the average values as the final atmospheric parameters for a given star. We estimated the final errors for each parameter by taking the average of the error values. We applied this procedure because the propagated standard deviation was too small and would underestimate the expected uncertainties. For example, in the case of the Young Sun candidates, the mean standard deviation for stars with at least three spectra was  $\approx 21$  K, 0.05 dex and 0.02 dex for  $T_{\text{eff}}$ ,  $\log g$  and  $[\text{Fe}/\text{H}]$ , respectively. For the SG candidates, the mean standard deviation for stars with at least three spectra was  $\approx 18$  K, 0.06 dex and 0.01 dex. These results reinforce the internal consistency of our atmospheric parameters, even though spectra from different instruments were used (see Section 2.2). This consistency is also illustrated in Figure 2, where the points representing the parameters for each spectrum are closely grouped for all stars.

We chose the star HD 146233 (18 Sco) as a control star in our sample in order to check the precision of our analysis during the project. Our derived atmospheric parameters for HD 146233 have a good agreement with previous works (e.g., G. Porto de Mello & L. da Silva 1997; M. Bazot et al. 2011; G. Porto de Mello et al. 2014; J. Meléndez et al. 2014; U. Heiter et al. 2015) as shown in Table 4.

We note that the choice of an analysis in 1D LTE does not affect the selection of the best candidates because the theoretical points ZAMS and SG both have parameters very close to the solar ones. Therefore, the 3D NLTE corrections for the parameter space studied in this work are  $A(X) \lesssim 0.03$  dex (e.g., A. M. Amarsi et al. 2022; K. Lind

**Table 3.** Final atmospheric parameters of all sample candidates. In order, the columns present: the star identification, its effective temperature, logarithm of the surface gravity, metallicity and the microturbulence velocity.

Star	$T_{eff}$ (K)	$\log g$ ( $cms^{-2}$ )	[ $Fe/H$ ] (dex)	$\xi$ ( $kms^{-1}$ )
Sun ZAMS	5586	4.53	0.00	–
HD 13531	$5634 \pm 17$	$4.54 \pm 0.04$	$-0.01 \pm 0.02$	$1.22 \pm 0.04$
HD 21411	$5482 \pm 17$	$4.53 \pm 0.04$	$-0.22 \pm 0.01$	$0.85 \pm 0.05$
HD 25918	$5528 \pm 25$	$4.45 \pm 0.06$	$-0.05 \pm 0.02$	$0.77 \pm 0.05$
HD 55720	$5503 \pm 21$	$4.45 \pm 0.09$	$-0.28 \pm 0.02$	$0.93 \pm 0.04$
HD 61033	$5639 \pm 25$	$4.55 \pm 0.06$	$0.02 \pm 0.02$	$1.12 \pm 0.05$
HD 64114	$5608 \pm 18$	$4.51 \pm 0.05$	$0.01 \pm 0.01$	$0.96 \pm 0.03$
HD 182619	$5557 \pm 27$	$4.49 \pm 0.08$	$-0.07 \pm 0.02$	$0.82 \pm 0.06$
HD 197210	$5581 \pm 19$	$4.52 \pm 0.04$	$0.01 \pm 0.01$	$0.88 \pm 0.04$
Sun SG	5743	4.18	0.00	–
HD 15942	$5934 \pm 11$	$4.45 \pm 0.06$	$0.43 \pm 0.01$	$1.13 \pm 0.03$
HD 19308	$5856 \pm 20$	$4.41 \pm 0.08$	$0.16 \pm 0.02$	$1.02 \pm 0.03$
HD 24040	$5821 \pm 21$	$4.29 \pm 0.05$	$0.20 \pm 0.02$	$1.10 \pm 0.04$
HD 69809	$5859 \pm 16$	$4.34 \pm 0.06$	$0.28 \pm 0.01$	$1.13 \pm 0.03$
HD 74698	$5792 \pm 16$	$4.25 \pm 0.04$	$0.12 \pm 0.01$	$1.08 \pm 0.03$
HD 111398	$5747 \pm 18$	$4.31 \pm 0.05$	$0.08 \pm 0.01$	$1.04 \pm 0.03$
HD 148577	$5725 \pm 29$	$4.22 \pm 0.09$	$-0.03 \pm 0.02$	$1.08 \pm 0.05$
HD 175425	$5871 \pm 45$	$4.38 \pm 0.11$	$0.15 \pm 0.03$	$1.13 \pm 0.08$
HD 196050	$5905 \pm 19$	$4.24 \pm 0.05$	$0.25 \pm 0.01$	$1.21 \pm 0.03$
HD 213575	$5680 \pm 16$	$4.18 \pm 0.04$	$-0.14 \pm 0.01$	$1.09 \pm 0.03$
Present Sun	5777	4.44	0.00	1.00
18 Sco	$5811 \pm 17$	$4.47 \pm 0.06$	$0.06 \pm 0.01$	$1.03 \pm 0.03$

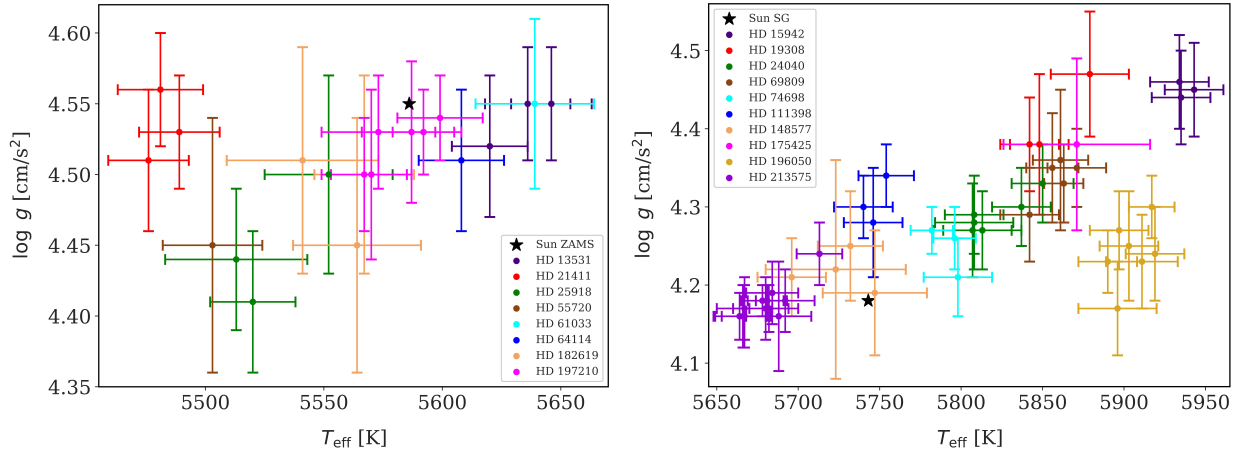


**Figure 2.** Effective temperatures  $T_{eff}$  and surface gravities  $\log g$  for all candidates. We present the ZAMS candidates in the left panel and the SG candidates in the right panel. Each unique color represents one of the candidates of the sample. The different values for same colored points represent the results obtained for each spectrum of the same star. The error bars show the respective uncertainties of each atmospheric parameter. The black stars represent the reference atmospheric parameters of the Sun at ZAMS and SG stages respectively.

& A. M. Amarsi 2024), a value that is within our uncertainties. Moreover, we compare each candidate's parameters with those from the corresponding theoretical point, making possible systematic effects negligible.

**Table 4.** Final atmospheric parameters of the solar twin HD 146233 (18 Sco) and comparison with previous works in the literature. In order, the columns present: the reference article, effective temperature, logarithm of the surface gravity, metallicity and the microturbulence velocity.

	$T_{eff}$ (K)	$\log g$ ( $cm s^{-2}$ )	[Fe/H] (dex)	$\xi$ ( $km s^{-1}$ )
This Work	$5811 \pm 17$	$4.47 \pm 0.06$	$0.06 \pm 0.01$	$1.03 \pm 0.03$
Bazot et al. (2011)	$5813 \pm 21$	$4.45 \pm 0.02$	$0.04 \pm 0.01$	-
Porto de Mello et al. (2014)	$5795 \pm 30$	$4.42 \pm 0.05$	$-0.03 \pm 0.04$	-
Meléndez et al. (2014)	$5823 \pm 6$	$4.45 \pm 0.02$	$0.05 \pm 0.01$	-
Gaia Benchmark Stars (2015)	$5786 \pm 30$	$4.39 \pm 0.07$	$0.03 \pm 0.01$	$1.20 \pm 0.20$

Atomic diffusion could, in principle, also affect the selection of the best candidates to represent the Sun throughout the main sequence because it can lower the surface iron abundance of solar-type stars due to gravitational settling by 0.1 dex (A. Dotter et al. 2017; B. Gustafsson 2025). However, we note that no candidate was excluded solely because of its metallicity (see Section 5), but rather due to a combination of its physical parameters (primarily age, which ruled out most of the SG candidates).

### 3.2. Chemical abundances

Using the atmospheric parameters from Section 3.1, we determined abundances of the following elements: carbon (C), oxygen (O), sodium (Na), magnesium (Mg), aluminum (Al), silicon (Si), calcium (Ca), titanium (Ti), nickel (Ni), chromium (Cr) and zinc (Zn). We used the code ARESV2 (S. Sousa et al. 2007, 2015) to automatically measure EWs for a list of lines with solar  $\log gf$  values that will be described in a future paper (Ghezzi et al., in prep.). In total, we measured 166 absorption lines from 11 different elements, spanning wavelengths from 4400 to 7800 Å; a spectral range covered by the majority of instruments used throughout this work. The determination of abundances was performed using the 2017 version of MOOG and the *abfind* task.

The abundance uncertainties for each element in each spectrum were estimated as follows: taking  $T_{eff}$  as an example, with its associated uncertainty  $\sigma_{T_{eff}}$  (as determined in Section 3.1), a new model atmosphere was computed using  $T_{eff} - \sigma_{T_{eff}}$ . All elemental abundances were recalculated, and the difference  $A(X)_{\text{new}} - A(X)_{\text{final}}$  was derived. The same procedure was repeated for  $T_{eff} + \sigma_{T_{eff}}$ , resulting in a pair of abundance deviations for each element. The maximum of the two values was adopted as the uncertainty due to  $T_{eff}$ . This process was repeated for the other atmospheric parameters:  $\log g$ , [Fe/H], and  $\xi$ . Finally, the total uncertainty in the abundance of each element was computed as the quadratic sum of five terms: the four contributions from the atmospheric parameters ( $T_{eff}$ ,  $\log g$ , [Fe/H], and  $\xi$ ) and the standard deviation of the mean of the final abundance measurements. This latter contribution was only considered for elements with two or more lines.

For the determination of O abundance, we utilized the O I triplet at 777 nm. However, it is well established in the literature that NLTE effects influence O abundance determinations in solar-type stars, on the order of a few tenths of a dex (D. Kiselman 2001). Briefly, 1D LTE analyzes of these O I lines tend to yield overestimated O abundances. To account for these NLTE effects, we applied the corrections derived by A. M. Amarsi et al. (2019).

We averaged the mean abundance of each element to obtain its final chemical abundance. The determined absolute abundances were subtracted from the solar reference abundances adopted from Table 1 of M. Asplund et al. (2009). Therefore, the abundance values presented here follow the notation [X/H], where X represents the element, and the abundance value is given in dex with its associated uncertainty, as presented in Table 5. Figure 3 shows the final chemical abundances of the best candidates in the sample (as it will be shown throughout the paper). The candidate HD 61033 shows an abundance pattern consistent with the solar reference, whereas HD 13531 is slightly more metal-poor than the Sun and HD 148577 is slightly more metal-rich. We performed linear fits for the abundances as a function of their condensation temperatures (taken from K. Lodders 2003), but found no statistically significant correlations for any of the candidates.

Note that the abundances of Ti and Cr are the weighted average between the values obtained from different ionization stages. We compared the abundances determined using Ti I/Ti II and Cr I/Cr II lines using weighted linear fits. The slopes were  $1.095 \pm 0.036$  and  $0.950 \pm 0.015$ , respectively, with  $R^2$  of 0.983 and 0.996. Additionally, the mean abundance difference (X I - X II) obtained between the ionized stages is  $-0.006 \pm 0.007$  dex for Ti, and  $-0.014 \pm 0.005$  dex for Cr. These results strengthen our confidence in the procedures adopted, as well as in the accuracy of the

atmospheric parameter determination carried out in Section 3.1. The abundances of Ti and Cr presented in Table 5 are also the weighted mean of the ionization stages.

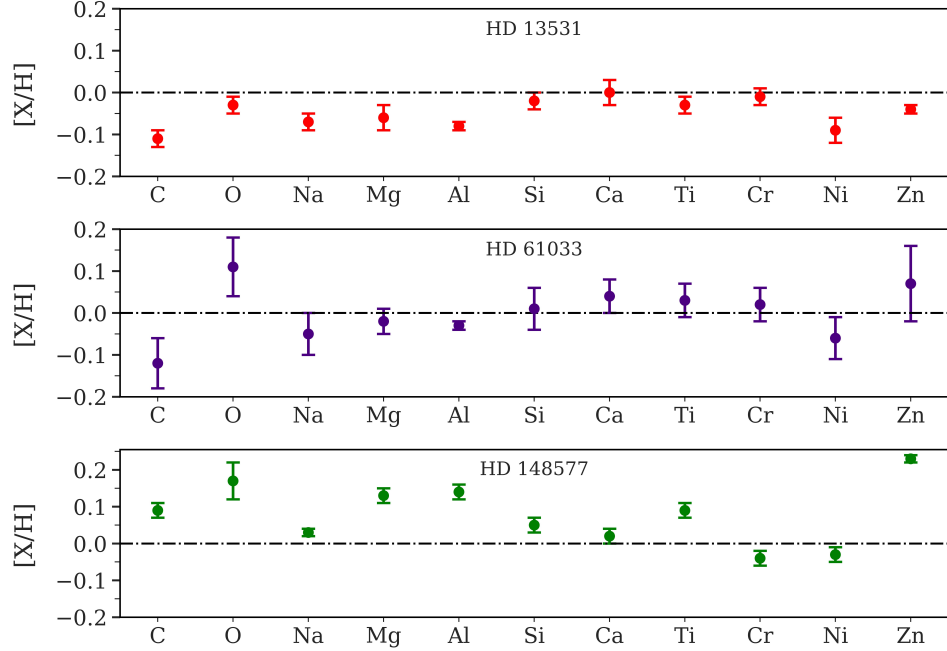


**Figure 3.** Chemical abundances for HD 13531 (ZAMS candidate; top panel), HD 61033 (ZAMS candidate; middle panel) and HD 148577 (SG candidate; lower panel). The dotted-dashed line marks the solar reference ( $[X/H] = 0.00$ ).

**Table 5.** Final chemical abundances ([X/H]) for all sample stars. The columns present the stellar ID followed by the abundance measurements (in dex) and their uncertainties for each chemical element. Weighted averages are shown for Cr and Ti.

Star	[C/H]	[O/H]	[Na/H]	[Mg/H]	[Al/H]	[Si/H]	[Ca/H]	[Ti/H]	[Cr/H]	[Ni/H]	[Zn/H]
HD 13531	-0.11 ± 0.02	-0.03 ± 0.02	-0.07 ± 0.02	-0.06 ± 0.03	-0.08 ± 0.01	-0.02 ± 0.02	0.00 ± 0.03	-0.03 ± 0.02	-0.01 ± 0.02	-0.09 ± 0.03	-0.04 ± 0.0
HD 21411	-0.21 ± 0.02	-	-0.29 ± 0.01	-0.19 ± 0.03	-0.23 ± 0.02	-0.21 ± 0.02	-0.17 ± 0.02	-0.18 ± 0.02	-0.20 ± 0.02	-0.28 ± 0.02	-0.23 ± 0.0
HD 25918	-0.14 ± 0.02	-	-0.22 ± 0.02	-0.04 ± 0.04	0.01 ± 0.02	-0.07 ± 0.02	-0.04 ± 0.03	-0.01 ± 0.02	-0.05 ± 0.02	-0.11 ± 0.02	-0.06 ± 0.0
HD 55720	-0.19 ± 0.04	-0.05 ± 0.05	-0.26 ± 0.05	-0.07 ± 0.06	-0.11 ± 0.05	-0.16 ± 0.03	-0.17 ± 0.05	-0.09 ± 0.03	-0.28 ± 0.04	-0.28 ± 0.04	-0.12 ± 0.0
HD 61033	-0.12 ± 0.06	0.11 ± 0.07	-0.05 ± 0.05	-0.02 ± 0.03	-0.03 ± 0.01	0.01 ± 0.05	0.04 ± 0.04	0.03 ± 0.04	0.02 ± 0.04	-0.06 ± 0.05	0.07 ± 0.09
HD 64114	-0.08 ± 0.04	-0.06 ± 0.04	-0.02 ± 0.06	0.06 ± 0.07	-0.01 ± 0.01	0.02 ± 0.03	0.02 ± 0.04	0.04 ± 0.03	0.01 ± 0.03	-0.02 ± 0.04	0.03 ± 0.06
HD 182619	-0.11 ± 0.04	-	-0.12 ± 0.02	-0.06 ± 0.04	-0.05 ± 0.02	-0.05 ± 0.02	-0.07 ± 0.03	-0.04 ± 0.02	-0.07 ± 0.02	-0.09 ± 0.02	-0.02 ± 0.0
HD 197210	-0.07 ± 0.01	-	-0.04 ± 0.02	0.01 ± 0.02	0.02 ± 0.02	0.00 ± 0.01	0.02 ± 0.01	0.02 ± 0.01	0.02 ± 0.01	-0.02 ± 0.01	0.03 ± 0.01
HD 15942	0.26 ± 0.02	-	0.49 ± 0.02	0.43 ± 0.03	0.42 ± 0.01	0.46 ± 0.02	0.40 ± 0.02	0.45 ± 0.02	0.44 ± 0.02	0.47 ± 0.02	0.56 ± 0.01
HD 19308	0.12 ± 0.02	-	0.22 ± 0.02	0.19 ± 0.02	0.19 ± 0.01	0.18 ± 0.02	0.10 ± 0.02	0.15 ± 0.02	0.16 ± 0.02	0.18 ± 0.02	0.16 ± 0.02
HD 24040	0.14 ± 0.02	0.21 ± 0.01	0.25 ± 0.01	0.20 ± 0.01	0.27 ± 0.01	0.23 ± 0.02	0.20 ± 0.02	0.24 ± 0.02	0.20 ± 0.02	0.23 ± 0.02	0.29 ± 0.01
HD 69809	0.26 ± 0.02	0.15 ± 0.02	0.43 ± 0.01	0.36 ± 0.02	0.34 ± 0.01	0.32 ± 0.02	0.24 ± 0.02	0.30 ± 0.02	0.29 ± 0.02	0.34 ± 0.01	0.23 ± 0.01
HD 74698	0.09 ± 0.02	-	0.07 ± 0.02	0.17 ± 0.03	0.16 ± 0.01	0.13 ± 0.02	0.12 ± 0.02	0.14 ± 0.02	0.12 ± 0.02	0.10 ± 0.02	0.21 ± 0.01
HD 111398	0.06 ± 0.02	-	0.06 ± 0.02	0.18 ± 0.02	0.19 ± 0.02	0.12 ± 0.02	0.09 ± 0.03	0.15 ± 0.02	0.09 ± 0.02	0.08 ± 0.02	0.23 ± 0.01
HD 148577	0.09 ± 0.02	0.17 ± 0.05	0.03 ± 0.01	0.13 ± 0.02	0.14 ± 0.02	0.05 ± 0.02	0.02 ± 0.02	0.09 ± 0.02	-0.04 ± 0.02	-0.03 ± 0.02	0.23 ± 0.01
HD 175425	0.11 ± 0.09	-	0.11 ± 0.06	0.15 ± 0.04	0.26 ± 0.03	0.17 ± 0.08	0.07 ± 0.05	0.20 ± 0.07	0.08 ± 0.05	0.14 ± 0.08	0.19 ± 0.02
HD 196050	0.21 ± 0.01	0.08 ± 0.02	0.39 ± 0.01	0.27 ± 0.01	0.30 ± 0.01	0.29 ± 0.01	0.23 ± 0.02	0.29 ± 0.01	0.26 ± 0.01	0.30 ± 0.01	0.40 ± 0.01
HD 213575	0.01 ± 0.01	-	-0.08 ± 0.01	0.06 ± 0.01	0.07 ± 0.01	-0.01 ± 0.01	-0.04 ± 0.01	0.04 ± 0.01	-0.13 ± 0.01	-0.13 ± 0.01	-0.02 ± 0.0

### 3.3. Evolutionary parameters

We obtained the evolutionary parameters (mass, radius, luminosity, and age) for every target star in our sample. This task was performed using the *isoclassify*<sup>7</sup> code (D. Huber et al. 2017; T. A. Berger et al. 2020) which compares observational parameters with grids of isochrones. We opted for the grid modeling mode of the code to derive the stellar parameters (for example, radius, mass, luminosity and age) which performs a direct integration of isochrones with a given set of observables as input (photometry, spectroscopy and parallax), generating posterior distributions for each stellar parameter. In our analysis of the sample, we chose to use the set of isochrones from the MESA Isochrones and Stellar Tracks (MIST) project (J. Choi et al. 2016; J. Choi et al. 2016). For the extinction calculation we chose the "all sky" option, which combines the reddening maps from J. Bovy et al. (2016) and *Bayestar19* (G. M. Green et al. 2019). However, it is important to note that we should not expect any major contribution from reddening and extinction in the photometry of our sample due to their proximity; our most distant candidate (HD 13531), excluding the control star, is located 26.13 pc away, as determined based on its parallax (38.27 mas). In fact, it was only possible to estimate this correction for 5 candidates, with the highest value  $A_V \approx 0.04$  (extinction in the  $V$  magnitude), almost negligible, as expected.

We also chose to provide the input parameters  $T_{eff}$ ,  $\log g$ , [Fe/H],  $V$  magnitude, celestial equatorial coordinates ( $RA$ ,  $DEC$ ) and parallax  $\pi$ , in addition to their respective uncertainties. The effective temperatures, the logarithm of the surface gravities and metallicities were determined spectroscopically in this work as described earlier (see Section 3.1). The  $RA$  and  $DEC$  coordinates and the parallaxes of the candidates, with their associated uncertainties, were collected from the second Data Release (DR2) of Gaia ( Gaia Collaboration et al. 2018). The  $V$  magnitudes were calculated using the following formula:  $V = V_T - [0.090(B_T - V_T)]$ ; the values of  $B_T$  and  $V_T$  were obtained from the *Tycho-2* catalog (E. Høg et al. 2000), for consistency with the data used during the selection of the sample, as described in Section 2. Uncertainties for the  $V$  magnitudes were determined through error propagation.

An example of the cumulative distribution functions (CDFs) for the evolutionary parameters fit for the ZAMS candidate HD 61033 can be seen in Figure 4. The individual values for the evolutionary parameters of each star in our sample can be seen in the Table 9. The distribution of masses, radii and ages for our sample show that we were capable of identifying interesting candidates to represent the Sun at ZAMS and SG stages as shown in Figure 5. Additionally, we included a Kernel Density Estimation (KDE) in the histograms of Figure 5, where their global peaks are located at  $0.96 M_\odot$ ,  $1.21 R_\odot$ , 3.71 Gyr for  $Age_{iso}$ , and 4.94 Gyr for  $Age_{HK}$  (see Section 4.1). As can be seen, the candidates HD 13531 and HD 61033 do not have ages consistent with the ZAMS stage; however, they are very close to the parameters expected for young solar analogs, and we will hereafter consider them as such.

### 3.4. Kinematics parameters

We also derived  $UVW$  components of the galactic space velocities for each star in our sample to check if their kinematics presented the expected behavior according to their evolutionary stage. To accomplish this we used the *gal\_uvw* code<sup>8</sup> from Astrolibpy package. This routine uses celestial equatorial coordinates ( $RA$ ,  $DEC$ ), proper motion on both coordinates ( $\mu_\alpha$  and  $\mu_\delta$ ), parallax ( $\pi$ ) and radial velocities ( $V_{rad}$ ) as input parameters to calculate the galactic components relative to the local standard of rest (LSR). All the input parameters were obtained from the second Data Release (DR2) of Gaia ( Gaia Collaboration et al. 2018). We adopted the code option of performing, at the end of the calculation, a correction relative to the solar components on the reference LSR, subtracting the  $UVW$  solar velocities, obtained by B. Coşkunoğlu et al. (2011), from the calculated velocities of each target star.

The  $UVW$  velocity components of our candidates can be seen in Table 6. It is important to note that the  $U$  component is positive towards the Galactic anticenter. The dispersion ellipses in the Figure 6 diagrams were created based on the work of M. C. Turnbull & J. C. Tarter (2003), in which velocity dispersions relative to the LSR were calculated for a significant sample of thin-disk stars with metallicity higher than  $-0.4$ . In general, we expect that ZAMS candidates should be more concentrated around the center of the dispersion ellipses, whereas SG candidates should exhibit greater dispersion in their components, which is what we observed in the diagrams of Figure 6.

## 4. STELLAR ACTIVITY AND AGE DIAGNOSTICS

Stellar age is a fundamental parameter to understand the evolutionary stage of a star and it appears to be correlated with its level of stellar activity. Furthermore, the latter can influence the atmospheres of exoplanets orbiting the star

<sup>7</sup> <https://github.com/danxhuber/isoclassify>

<sup>8</sup> [https://github.com/segasai/astrolibpy/blob/master/astrolib/gal\\_uvw.py](https://github.com/segasai/astrolibpy/blob/master/astrolib/gal_uvw.py)

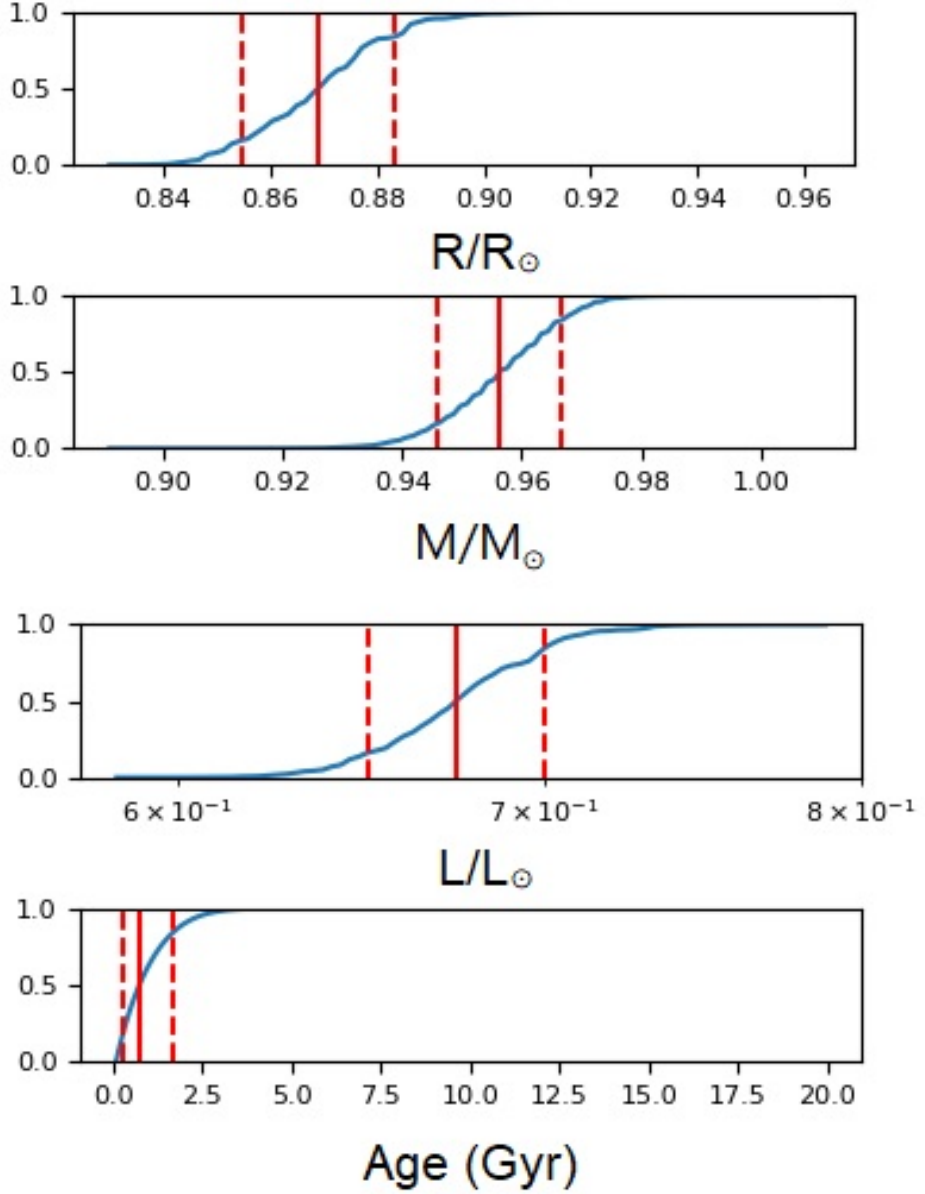


**Figure 4.** The output of the isoclassify code for the ZAMS candidate HD 61033. From the upper to lower panels we have the fits for the radius, mass, luminosity and age, respectively. The blue line represents the cumulative distribution function, while the solid red line represents the best value fitted. The dashed red lines represent uncertainties for the best value.

and their habitability, potentially affecting the retention of a sufficiently dense atmosphere due to atmospheric erosion processes (M. W. Powne et al. 2009; I. Ribas et al. 2010; J. Krissansen-Totton et al. 2024), or even the development of conditions necessary for life as we know it. Therefore, an accurate determination of the stellar age is an essential parameter for a better understanding of the evolutionary scenario of the star and its system. The isochronal method (used in Section 3.3) has limitations, for example, in the ZAMS region the isochrones are close to each other resulting in a wider range of possible age solutions for a given set of input parameters. With respect to older stars, particularly the SG candidates, the isochrone method performs effectively due to the increased spacing between the isochrone curves, which facilitates an accurate age estimation. With that in mind, we decided to use other indicators, so we can estimate ages more accurately and better evaluate the evolutionary stage of each target star.

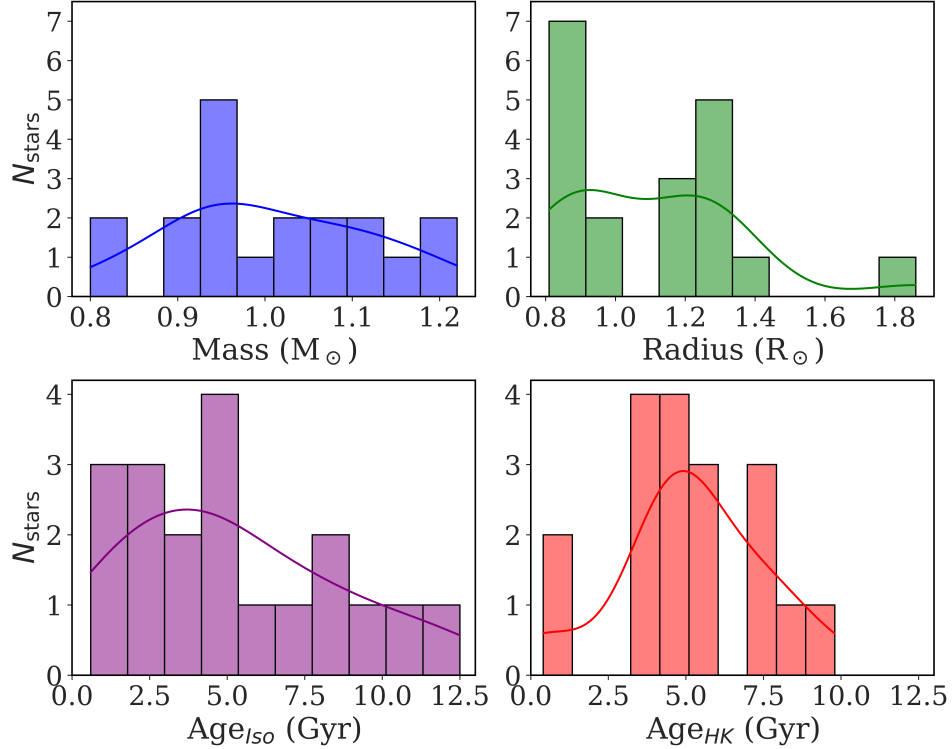


**Figure 5.** Distribution of stellar parameters for the entire sample. The panels show histograms of stellar mass, radius, and two age estimates (from isochrone fitting,  $\text{Age}_{\text{Iso}}$ , and from chromospheric activity,  $\text{Age}_{\text{HK}}$ ). The y-axis in all panels represents the number of stars in each bin. A kernel density estimate (KDE) is overplotted to highlight the underlying distribution trends.

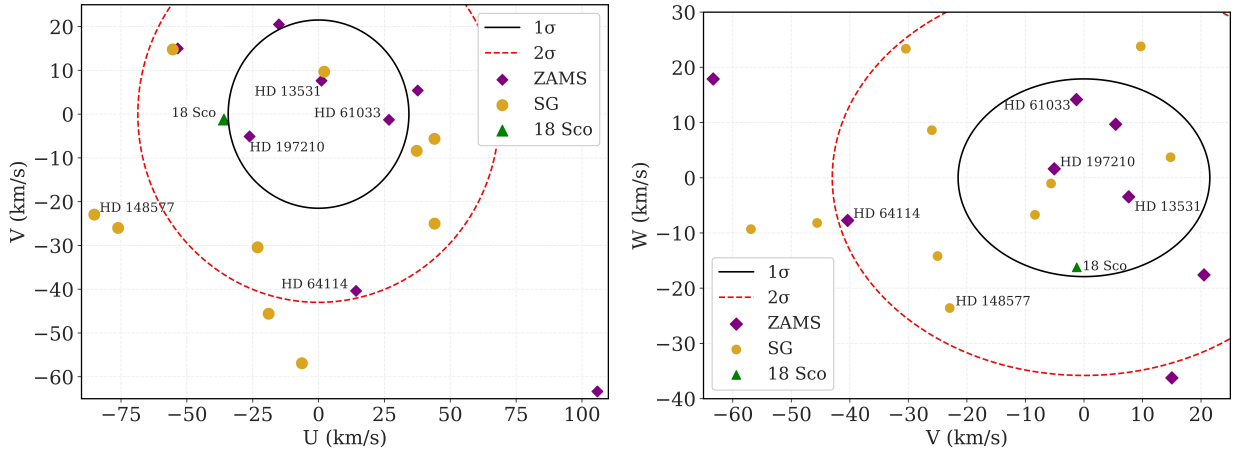


**Figure 6.** On the left panel, we present the diagram of the  $U \times V$  components, while on the right panel, we show the diagram for the  $V \times W$  components. The velocity dispersion ellipses for each component, with semi-major axes of  $1\sigma$  and  $2\sigma$ , are represented by the solid black and dashed red lines, respectively. They were constructed based on the work of [M. C. Turnbull & J. C. Tarter \(2003\)](#) and  $\sigma$  values are:  $\sigma_U = 34.3 \text{ km s}^{-1}$ ,  $\sigma_V = 21.5 \text{ km s}^{-1}$  and  $\sigma_W = 17.9 \text{ km s}^{-1}$ . The purple diamonds represent the values of the ZAMS candidates, while the golden dots represent the SG candidates. Our control star 18 Sco is represented by the green triangle. The labeled stars are discussed in further detail throughout the article.

#### 4.1. $\text{Ca II H \& K}$ lines

The Ca II H & K lines can be good tracers for the age of a star because of their sensitivity to the star's chromospheric activity. The chromospheric flux contribution in these spectral lines can be measured using the S index ([A. H. Vaughan et al. 1978](#); [F. Middelkoop 1982](#)), which is the ratio of the flux in the line cores of the Ca II H (3968.17Å) & K (3933.66Å)

**Table 6.** Final kinematic parameters of the sample candidates. The columns in the table represent: star, stage to which it is a candidate and velocity components U, V and W, respectively.

Star	U $km s^{-1}$	V $km s^{-1}$	W $km s^{-1}$
HD 13531	1.125	7.630	-3.455
HD 21411	37.634	5.411	9.686
HD 25918	-53.469	15.012	-36.228
HD 55720	105.849	-63.345	17.890
HD 61033	26.705	-1.292	14.159
HD 64114	14.226	-40.385	-7.725
HD 182619	-15.058	20.503	-17.588
HD 197210	-26.206	-5.089	1.619
HD 15942	37.259	-8.382	-6.709
HD 19308	44.017	-25.016	-14.174
HD 24040	-18.968	-45.585	-8.172
HD 69809	2.115	9.697	23.795
HD 74698	-23.148	-30.433	23.370
HD 111398	-55.336	14.797	3.713
HD 148577	-85.143	-22.943	-23.580
HD 175425	-6.319	-56.903	-9.298
HD 196050	-76.096	-25.995	8.627
HD 213575	43.987	-5.636	-1.035
18 Sco	-35.926	-1.238	-16.214

lines and two nearby pseudo-continuum regions (3991.07 and 4011.07Å). The S index can be used to obtain the  $\log R'_{HK}$  of each candidate, through proper flux calibration and photospheric correction, procedures that will be described in the next paragraphs. The  $\log R'_{HK}$  is the standard metric in the literature and we can apply activity-age relations to estimate the age of the candidates (e.g., [D. Lorenzo-Oliveira et al. 2016](#)).

We used a code that compiles a database of S indexes from a variety of sources: [T. J. Henry et al. \(1996\)](#); [R. O. Gray et al. \(2003\)](#); [J. T. Wright et al. \(2004\)](#); [R. Gray et al. \(2006\)](#); [J. Jenkins et al. \(2008\)](#); [H. Isaacson & D. Fischer \(2010\)](#); [P. Arriagada \(2011\)](#) and [J. S. Jenkins et al. \(2011\)](#). Nonetheless, we gave priority to [H. Isaacson & D. Fischer \(2010\)](#) and [J. T. Wright et al. \(2004\)](#) surveys because they were constructed based on years of time series with the HIRES/Keck spectrograph. For stars present in both of these catalogs, we adopted the average value. If they were present in neither of these surveys, the code returns the median value found on the other surveys. For the control star, HD 146233, we adopted the S index derived by [D. Lorenzo-Oliveira et al. \(2018\)](#) through long-term monitoring of its chromospheric cycle.

Finally, we converted the S indexes to  $\log R'_{HK}$  following the procedures described in [R. Rutten \(1984\)](#) and [F. Middelkoop \(1982\)](#). In summary, the S index is affected by the spectral type of the star, as the measurement depends on the nearby continuum regions. Therefore, a correction must be applied to remove this effect ([F. Middelkoop 1982](#)). Additionally, it is necessary to eliminate the photospheric contribution ( $R_{phot}$ ) present at the center of these lines within the spectral measurement window. The  $\log R'_{HK}$  index of each star is shown as a function of their (B-V) values in the Figure 7. The (B-V) color values for each candidate were obtained from the Hipparcos catalog ([M. A. Perryman et al. 1997](#)). With the  $\log R'_{HK}$  estimated, we applied the age-mass-metallicity-activity relation from [D. Lorenzo-Oliveira et al. \(2016\)](#) to obtain the ages of our target stars, which is represented by the equation below:

$$\log(\text{Age}_{HK}) = -56.01 - 25.81 \cdot \log(R'_{HK}) - 0.436 \cdot [\text{Fe}/\text{H}] - 1.26 \cdot \log(M/M_{\odot}) - 2.529 \cdot \log(R'_{HK})^2. \quad (1)$$

The values adopted for the metallicity and mass were retrieved from Tables 3 and 9, respectively. The individual results for the chromospheric age can be seen in Table 8. As can be seen in Table 7 and Figure 7, the target stars HD 13531 and HD 61033 are very active and young, turning them into promising candidates to represent the young Sun, very similar to  $\kappa^1$  Cet ([I. Ribas et al. 2010](#)), but less active and older when compared to the ZAMS analog EK

Dra (M. Güdel et al. 1997). Furthermore, all other ZAMS candidates exhibit chromospheric activity levels below the threshold required to be classified as active, except for HD 21411, which lies precisely at the threshold ( $\log R'_{HK} = -4.75$ ). Moreover, our best candidate for the SG stage (HD 148577) presents lower levels of chromospheric activity, which is consistent with older stars. Additionally, all the SG candidates are less active than the Sun, as expected, with the exception of the candidate HD 175425.

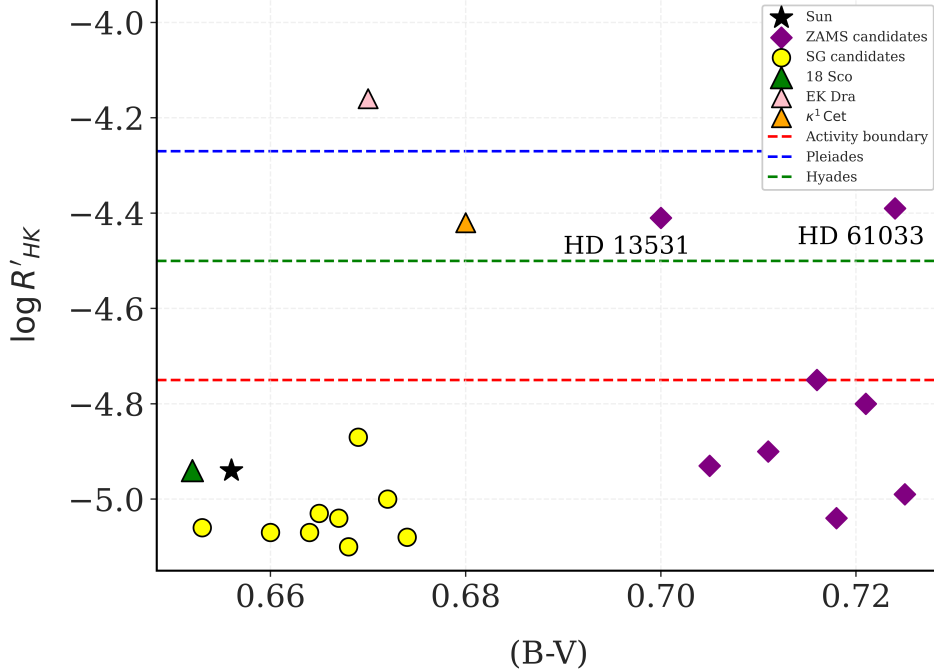


**Figure 7.** Chromospheric activity indicator  $\log R'_{HK}$  as a function of (B-V) for all stars in the sample. The purple diamonds represent the values of the ZAMS candidates, while the yellow points represent the SG candidates. Our control star 18 Sco is represented by the green triangle ( $\log R'_{HK} = -4.94$ , as derived in Section 4.1). The black star represents the values adopted for the Sun for comparison ( $\log R'_{HK} = -4.94$ ; D. Lorenzo-Oliveira et al. 2018). The red dashed line represents the value of  $\log R'_{HK} = -4.75$  that was used as boundary to separate the active stars of the sample from the inactive ones (T. J. Henry et al. 1996). The blue and green dashed lines show the average values for the Pleiades ( $\log R'_{HK} = -4.27$ ) and Hyades ( $\log R'_{HK} = -4.50$ ) active groups, respectively, derived by E. E. Mamajek & L. A. Hillenbrand (2008) for comparison. We also show the  $\log R'_{HK}$  values for the young sun analogs  $\kappa^1$  Cet ( $\log R'_{HK} = -4.42$ ) and EK Dra ( $\log R'_{HK} = -4.16$ ) as the pink and orange triangles, respectively, from E. L. Brown et al. (2022) and E. E. Mamajek & L. A. Hillenbrand (2008).

#### 4.2. The $H\alpha$ line

Another interesting chromospheric indicator is the  $H\alpha$  line ( $\lambda = 6562.8$  Å). Although chromospheric radiative losses are weaker in this line compared to the H & K lines (L. Pasquini & R. Pallavicini 1991), which can lead to higher relative uncertainties,  $H\alpha$  fluxes have the advantage of being less affected by stellar magnetic cycles and transient phenomena such as flares and starspots (W. Lyra & G. F. Porto de Mello 2005). These phenomena can cause variations in  $\log R'_{HK}$ , even in very inactive stars (J. Gomes da Silva et al. 2021). We compiled  $H\alpha$  chromospheric fluxes ( $\text{erg cm}^{-2} \text{ s}^{-1}$ ) for our sample stars following P. V. Souza dos Santos et al. (2024), who used atmospheric models and medium-resolution spectra. They also constructed an age-mass-metallicity-activity relation, expressed as:

$$\log(\text{Age}_{H\alpha}) = -107.306 + 42.976 \cdot \log(F'_{H\alpha}) - 4.279 \cdot \log(M/M_\odot) + 0.835 \cdot [\text{Fe}/\text{H}] - 3.931 \cdot \log(F'_{H\alpha})^2. \quad (2)$$

Their published chromospheric fluxes and ages are presented in Table 8, along with the corresponding uncertainties. The high  $H\alpha$  chromospheric activity levels of HD 13531 and HD 61033, the only stars with  $F'_{H\alpha} > 10^6 \text{ erg cm}^{-2} \text{ s}^{-1}$ , reinforce their youth. Among the subgiant candidates, all of them present  $F'_{H\alpha} < 10^6 \text{ erg cm}^{-2} \text{ s}^{-1}$ , which is compatible with the hypothesis that they should have lower chromospheric activity levels.

**Table 7.** Chromospheric age and input parameters used in the calculation. In order, the columns are: S index compiled from various literature sources (see Section 4.1), the (B-V) color of each candidate.

Star	$\langle S_{MW} \rangle$	$(B - V)$	$\log R'_{HK}$
HD 13531	$0.386 \pm 0.005$	0.700	-4.41
HD 21411	$0.224 \pm 0.017$	0.716	-4.75
HD 25918	$0.165 \pm 0.005$	0.725	-4.99
HD 55720	0.175	0.705	-4.93
HD 61033	$0.409 \pm 0.029$	0.724	-4.39
HD 64114	$0.21 \pm 0.01$	0.721	-4.80
HD 182619	$0.156 \pm 0.001$	0.718	-5.04
HD 197210	0.183	0.711	-4.90
HD 15942	-	-	-
HD 19308	$0.160 \pm 0.004$	0.672	-5.00
HD 24040	$0.150 \pm 0.003$	0.653	-5.06
HD 69809	$0.148 \pm 0.002$	0.674	-5.08
HD 74698	0.156	0.665	-5.03
HD 111398	$0.150 \pm 0.002$	0.660	-5.07
HD 148577	0.152	0.664	-5.07
HD 175425	0.185	0.669	-4.87
HD 196050	0.154	0.667	-5.04
HD 213575	$0.146 \pm 0.001$	0.668	-5.10
18 Sco	$0.170 \pm 0.004$	0.652	-4.94

**Table 8.** In order, the columns are: the star identification, its proposed evolutionary stage, the  $H\alpha$  flux  $F'_{H\alpha}$  and its uncertainty in  $\text{erg cm}^{-2} \text{ s}^{-1}$ , the estimated age using  $H\alpha$  activity relation (Age  $H\alpha$ ), the age derived from the  $\log R'_{HK}$  index (Age  $HK$ ), and the age from isochrone fitting (Age  $Iso$ ) and their respective uncertainties. All age estimates are presented in gigayear units.

ID	$F'_{H\alpha}$ ( $\text{erg cm}^{-2} \text{ s}^{-1}$ )	$\sigma(F'_{H\alpha})$ ( $\text{erg cm}^{-2} \text{ s}^{-1}$ )	Age $_{H\alpha}$ (Gyr)	Age $_{HK}$ (Gyr)	Age $_{Iso}$ (Gyr)
HD 13531	1.230E+06	1.588E+05	$0.576^{+0.425}_{-0.245}$	$0.4^{+0.2}_{-0.1}$	$0.6^{+0.7}_{-0.4}$
HD 21411	7.563E+05	1.426E+05	$4.440^{+3.276}_{-1.885}$	$5.0^{+1.9}_{-1.4}$	$4.5^{+0.9}_{-0.9}$
HD 25918	4.474E+05	1.271E+05	$15.852^{+11.695}_{-6.730}$	$7.4^{+2.9}_{-2.0}$	$8.1^{+1.3}_{-1.4}$
HD 55720	5.227E+05	1.424E+05	$10.778^{+7.952}_{-4.576}$	$9.8^{+3.7}_{-2.7}$	$12.5^{+1.5}_{-1.5}$
HD 61033	1.599E+06	1.635E+05	$0.167^{+0.123}_{-0.071}$	$0.4^{+0.1}_{-0.1}$	$0.7^{+0.9}_{-0.5}$
HD 64114	6.586E+05	1.471E+05	$7.098^{+5.237}_{-3.014}$	$4.1^{+1.5}_{-1.1}$	$2.1^{+0.8}_{-0.8}$
HD 182619	6.803E+05	1.304E+05	$5.943^{+4.385}_{-2.523}$	$7.9^{+2.9}_{-2.2}$	$6.0^{+1.5}_{-1.6}$
HD 197210	9.040E+05	1.484E+05	$2.223^{+1.640}_{-0.944}$	$5.5^{+2.1}_{-1.5}$	$2.4^{+0.8}_{-0.7}$
HD 15942	5.170E+05	1.459E+05	$9.243^{+6.819}_{-3.924}$	-	$1.3^{+0.3}_{-0.4}$
HD 19308	5.599E+05	1.471E+05	$7.558^{+5.576}_{-3.209}$	$4.8^{+1.8}_{-1.3}$	$3.9^{+0.6}_{-0.6}$
HD 24040	8.554E+05	1.569E+05	$2.138^{+1.577}_{-0.908}$	$4.6^{+1.7}_{-1.3}$	$5.3^{+0.6}_{-0.4}$
HD 69809	6.988E+05	1.537E+05	$4.228^{+3.119}_{-1.795}$	$4.1^{+1.6}_{-1.1}$	$3.8^{+0.3}_{-0.3}$
HD 74698	3.895E+05	1.366E+05	$13.350^{+9.850}_{-5.668}$	$5.2^{+2.0}_{-1.4}$	$7.3^{+0.3}_{-0.3}$
HD 111398	5.565E+05	1.489E+05	$7.813^{+5.764}_{-3.317}$	$5.8^{+2.2}_{-1.6}$	$7.9^{+0.4}_{-0.4}$
HD 148577	5.830E+05	1.549E+05	$7.117^{+5.251}_{-3.022}$	$7.0^{+2.6}_{-2.0}$	$9.8^{+0.6}_{-0.6}$
HD 175425	6.393E+05	1.482E+05	$5.337^{+3.938}_{-2.266}$	$3.7^{+1.4}_{-1.0}$	$4.8^{+0.9}_{-0.9}$
HD 196050	6.800E+05	1.609E+05	$3.964^{+2.925}_{-1.683}$	$4.0^{+1.6}_{-1.1}$	$4.2^{+0.2}_{-0.4}$
HD 213575	5.406E+05	1.454E+05	$6.457^{+4.764}_{-2.741}$	$8.0^{+3.1}_{-2.2}$	$11.1^{+0.3}_{-0.3}$
HD 146233	6.159E+05	1.583E+05	$5.702^{+4.207}_{-2.421}$	$5.1^{+1.9}_{-1.4}$	$2.3^{+0.6}_{-0.5}$

### 4.3. *TESS* light curves

The TESS (Transiting Exoplanet Survey Satellite/NASA<sup>9</sup>, G. R. Ricker et al. 2010) mission provides valuable photometric data for determining rotation periods of magnetically active stars. By delivering high-precision, short-cadence light curves, TESS enables the detection of rotational modulation caused by surface inhomogeneities, such as star spots. This technique is particularly effective for stars with strong magnetic activity, where the modulation amplitude is more pronounced, as illustrated by HD 13531 in Figure 8 (upper panel). The continuous coverage of  $\sim 27$  days per sector allows the reliable determination of rotation periods, particularly for spot-dominated stars with moderate to rapid rotation ( $P_{\text{rot}} \lesssim 15$  days). According to standard gyrochronology relations (e.g., S. A. Barnes 2007; E. E. Mamajek & L. A. Hillenbrand 2008), a single Sun-like star with  $P_{\text{rot}} \simeq 15$  days typically corresponds to an age between 1.5 and 2.5 Gyr. Therefore, photometric rotation periods could be only derived for the youngest and most active stars in our sample: HD 13531 and HD 61033.

We obtained their light curves using the *lightkurve* package (Lightkurve Collaboration et al. 2018), and applied three independent techniques to estimate the rotation period: Lomb Scargle (J. T. VanderPlas 2018), an auto-correlation function (T. Reinhold & S. Hekker 2020) and the Phase dispersion minimization method (PDM; I. Jurkevich 1971; R. F. Stellingwerf 1978). In addition, we estimated their ages using the *gyrointerp* package and their gyrochrones (L. G. Bouma et al. 2023). All the TESS data used in this paper can be found in MAST 2021: <https://doi.org/10.17909/t9-nmc8-f686> - Sectors: 7, 8, 9, 18, 34, 35, 36, 58, 85.

Figure 8 shows, in the upper panel, the TESS light curve of the active star HD 13531. In the lower panel, we present the PDM analysis, where the green curve shows the theta values for different periods, which represent the variance within the phase bins. The period that minimizes theta corresponds to the true rotational period, indicated by the black line around 7.6 days. This result is consistent with the 7.5-day period reported in the GCVS catalog (N. N. Samus' et al. 2017) and also with the stellar ages estimated from the Ca II H & K activity index, the H $\alpha$  method and the isochronal method (0.4, 0.576 and 0.6 Gyr, respectively). The ACF method yielded a rotation period of approximately 6.02 days, consistent with a young and active star. In addition, the Lomb-Scargle periodogram identified a strong signal at 3.74 days, which is likely a harmonic of the true  $\approx$ 7-day rotational period.

<sup>9</sup> <https://science.nasa.gov/mission/tess/>

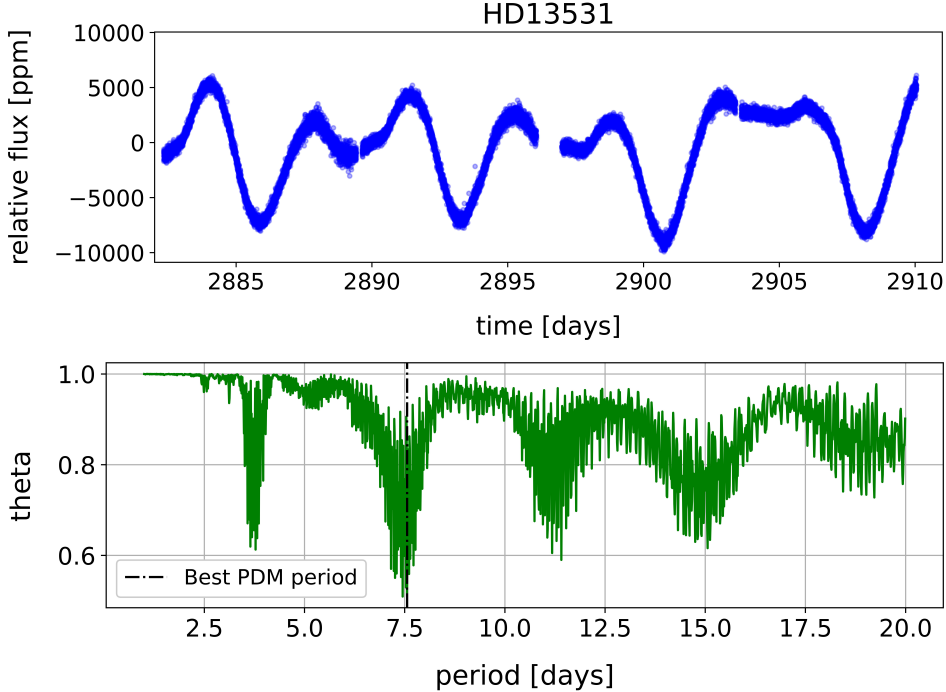


**Figure 8.** In the top pannel, the light curve that was used to determine the rotation period of the star HD 13531. In the bottom panel, the minimum value for theta obtained from the PDM method (phase dispersion minimization; [I. Jurkevitch 1971](#); [R. F. Stellingwerf 1978](#)) is shown, corresponding to  $P_{rot} = 7.6$  days.

For the star HD 61033, another active candidate, the three methods used provide an average of  $P_{rot} = 7.31 \pm 0.01$ . This value is compatible with a very active star, around 0.5 Gyr, a value compatible with its chromospheric and isochronal ages. In Figure 9 we present the final fit for the estimated ages using the mean value estimated by the three methods. For comparison, in Figure 9 we also present the rotational period of the young sun analogs  $\kappa^1$  Cet (8.77 days - [G. A. H. Walker et al. 2007](#); [I. Ribas et al. 2010](#)) and EK Dra (2.68 days - [M. Güdel et al. 1997](#)). The rotational period and age of our young sun candidates reinforce their candidacy, both of them are similar to  $\kappa^1$  Cet, however, older (and more evolved) than EK Dra.

## 5. BEST CANDIDATES

Throughout Sections 3 and 4, we have performed a very detailed characterization of the candidates in our sample. Now, we will use the previous results to define which stars can be selected as interesting candidates to represent the Sun at different stages.

### 5.1. Young Sun analogs

The consistency between the parameters of the ZAMS candidates and the reference solar values at this stage can be seen in Table 10. The candidates HD 13531 and HD 61033 are excellent candidates to represent the young Sun.

The star HD 13531 is one of the best candidates of our sample. Its atmospheric and evolutionary parameters are close to those adopted as reference values in this work within  $2\sigma$ . It exhibits chemical abundances close to solar values when the associated uncertainties are taken into account. The average abundance difference,  $\Delta[X/H]$ , was  $-0.0493 \pm 0.035$ . Its components of the Galactic space velocities are consistent with those of a young star. We observed a strong chromospheric emission at the centers of the Ca II H & K lines, which is in agreement with the indexes found in the literature ([J. T. Wright et al. 2004](#); [H. Isaacson & D. Fischer 2010](#)), and also confirmed by our estimated  $\log R'_{HK}$  value. Furthermore, this candidate exhibits an  $F'_{H\alpha}$  that is consistent with a young and active star. Finally, we estimate its age through 4 different methods, and we obtained a  $1\sigma$  agreement between them, which are compatible with the values expected for a young solar analog. Its derived rotational period ( $P_{rot} = 6.81$  days) is consistent with our age estimates for this candidate, reinforcing its youth.

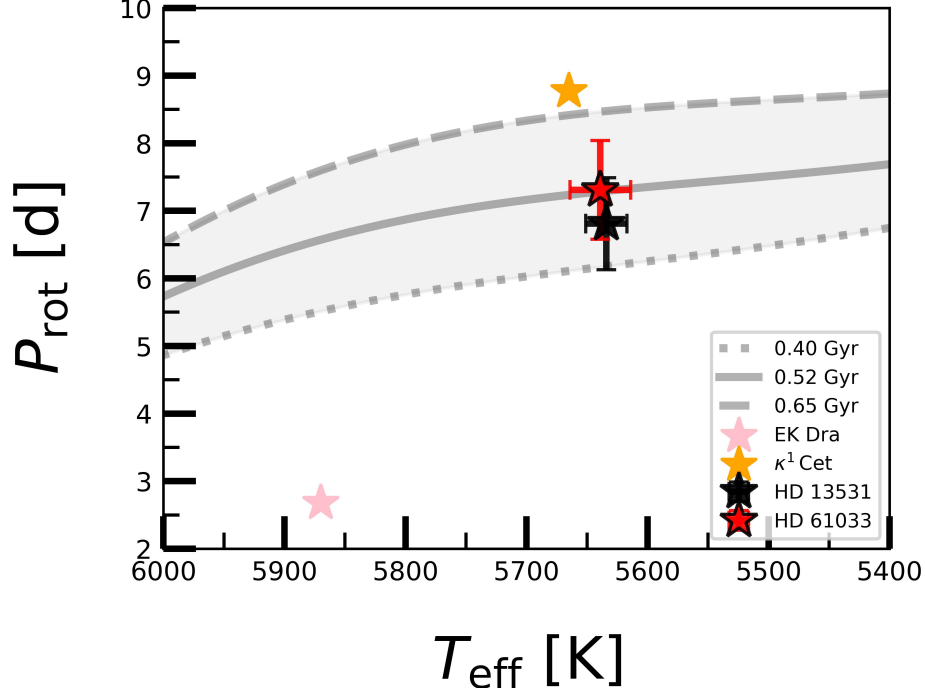


**Figure 9.** Rotation period ( $P_{\text{rot}}$ ) as a function of effective temperature ( $T_{\text{eff}}$ ) for the candidate stars. The grey lines represent gyrochrones for different ages: 0.40 Gyr (dotted), 0.52 Gyr (solid), and 0.65 Gyr (dashed). The black and red stars correspond to HD 13531 and HD 61033, respectively. Error bars reflect the uncertainties in both  $T_{\text{eff}}$  and  $P_{\text{rot}}$  measurements. The pink and orange stars represent EK Dra and  $\kappa^1$  Cet respectively, with  $T_{\text{eff}}$  and  $P_{\text{rot}}$  adopted from [I. Ribas et al. 2010](#) and [M. Güdel et al. 1997](#).

The candidate HD 61033 is a very active star, with  $\log R'_{HK} = -4.39$ , and its estimated rotational period ( $P_{\text{rot}} = 7.31 \pm 0.01$  days) is compatible with this value. Besides these factors, its atmospheric and evolutionary parameters are very close, within  $2\sigma$  for almost every parameter, to those adopted for the ZAMS Sun. The candidate HD 61033 presents chemical abundances that are consistent with solar values within the uncertainties. The average  $\Delta[\text{X}/\text{H}]$  for this candidate is  $-0.001 \pm 0.063$ . Its age indicators also point to a young star ( $\approx 0.3\text{-}0.5$  Gyr), which turns it into one, if not the most, promising candidates in the sample. Its  $\text{Age}_{H\alpha}$  estimate indicates an even younger candidate (0.167 Gyr), slightly older than the Pleiades Cluster ([A. Prša et al. 2016](#)). This star would thus be one of our best candidates. However, during the course of this work, the candidate HD 61033 was identified as a spectroscopic binary ([Barbato, D. et al. 2023](#)). Its companion is a  $0.32M_{\odot}$  star in an orbit with a semi-major axis of 0.91AU.

We note that the candidate HD 13531 has ages of  $\approx 0.3\text{-}0.5$  Gyr, which places it as interesting target to study the conditions present on the planetary system at the epoch when life arose on Earth (Archaeon Eon). These conditions are critical to the development of Earth's primitive atmosphere and the development of life itself. In addition, the candidate HD 197210 is quite interesting for the study of Sun-like stars, however, a little more evolved past the ZAMS, close to the age of 2.0 Gyr, when oxygen became significantly abundant in Earth's atmosphere.

### 5.2. Subgiant stage

The star HD 148577 has a marginally lower mass and higher metallicity than the Sun. Its effective temperature and surface gravity are inside the  $1\sigma$  interval around the theoretical point defined for the SG Sun. Its abundances are consistent with solar values within the uncertainties, with an average  $\Delta[\text{X}/\text{H}]$  of  $0.0791 \pm 0.0835$ . Its isochronal age is consistent with expectations for a star at this stage, while its chromospheric age is also relatively high, but lower than the isochronal estimate. This is confirmed by the nearly identical age estimates from ( $\text{Age}_{H\alpha}$ ) and ( $\text{Age}_{HK}$ ), indicating that this candidate is indeed fairly inactive and evolved, as expected, however, at a stage prior to the turnoff. We know that determining a precise chromospheric age for evolved stars is difficult, mainly due to the abrupt drop in chromospheric activity as stars evolve. [D. Lorenzo-Oliveira et al. \(2016\)](#) showed that this type of analysis can be done

**Table 9.** Final evolutionary parameters for all the candidates. In order, the columns are: the star identification, the extinction in the V band  $A_V$  in magnitudes, the stellar mass  $M$  in solar units, the stellar radius  $R$  in solar units, the stellar luminosity  $L$  in solar units, the age derived from isochrone fitting ( $Age_{iso}$ ), the age derived from the  $\log R'_{HK}$  index ( $Age_{HK}$ ), the age estimated from the  $H\alpha$  activity relation ( $Age_{H\alpha}$ ), and the age determined from stellar rotation ( $Age_{Rot}$ ). All age estimates are given in gigayears units.

Star	$A_V$ (mag)	$M$ ( $M_\odot$ )	$R$ ( $R_\odot$ )	$L$ ( $L_\odot$ )	$Age_{iso}$ (Gyr)	$Age_{HK}$ (Gyr)	$Age_{H\alpha}$ (Gyr)	$Age_{Rot}$ (Gyr)
Sun ZAMS	-	1.00	0.90	0.70	0.0	0.0	0.0	0.0
HD 13531	-	$0.95^{+0.01}_{-0.01}$	$0.86^{+0.01}_{-0.01}$	$0.66^{+0.01}_{-0.01}$	$0.6^{+0.7}_{-0.4}$	$0.4^{+0.2}_{-0.1}$	$0.576^{+0.425}_{-0.245}$	0.47
HD 21411	-	$0.84^{+0.01}_{-0.01}$	$0.81^{+0.01}_{-0.01}$	$0.52^{+0.01}_{-0.01}$	$4.5^{+0.9}_{-0.9}$	$5.0^{+1.9}_{-1.4}$	$4.440^{+3.276}_{-1.885}$	-
HD 25918	-	$0.89^{+0.01}_{-0.01}$	$0.93^{+0.02}_{-0.02}$	$0.72^{+0.02}_{-0.02}$	$8.1^{+1.3}_{-1.4}$	$7.4^{+2.9}_{-2.0}$	$15.852^{+11.695}_{-6.730}$	-
HD 55720	0.019	$0.80^{+0.01}_{-0.01}$	$0.89^{+0.02}_{-0.01}$	$0.66^{+0.02}_{-0.02}$	$12.5^{+1.5}_{-1.5}$	$9.8^{+3.7}_{-2.7}$	$10.778^{+7.952}_{-4.576}$	-
HD 61033	0.028	$0.96^{+0.01}_{-0.01}$	$0.87^{+0.01}_{-0.01}$	$0.67^{+0.03}_{-0.02}$	$0.7^{+0.9}_{-0.5}$	$0.4^{+0.1}_{-0.1}$	$0.167^{+0.123}_{-0.071}$	0.52
HD 64114	-	$0.95^{+0.01}_{-0.01}$	$0.89^{+0.01}_{-0.01}$	$0.70^{+0.01}_{-0.03}$	$2.1^{+0.8}_{-0.8}$	$4.1^{+1.5}_{-1.1}$	$7.098^{+5.237}_{-3.014}$	-
HD 182619	0.024	$0.90^{+0.01}_{-0.01}$	$0.90^{+0.01}_{-0.01}$	$0.69^{+0.02}_{-0.02}$	$6.0^{+1.5}_{-1.6}$	$7.9^{+2.9}_{-2.2}$	$5.943^{+4.385}_{-2.523}$	-
HD 197210	-	$0.94^{+0.01}_{-0.01}$	$0.88^{+0.01}_{-0.01}$	$0.67^{+0.01}_{-0.01}$	$2.4^{+0.8}_{-0.7}$	$5.5^{+2.1}_{-1.5}$	$2.223^{+1.640}_{-0.944}$	-
Sun SG	-	1.00	1.34	1.76	10.0	10.0	10.0	10.0
HD 15942	-	$1.22^{+0.01}_{-0.01}$	$1.19^{+0.02}_{-0.02}$	$1.57^{+0.05}_{-0.04}$	$1.3^{+0.3}_{-0.4}$	-	$9.243^{+6.819}_{-3.924}$	-
HD 19308	-	$1.08^{+0.02}_{-0.01}$	$1.13^{+0.02}_{-0.02}$	$1.34^{+0.04}_{-0.04}$	$3.9^{+0.6}_{-0.6}$	$4.8^{+1.8}_{-1.3}$	$7.558^{+5.576}_{-3.209}$	-
HD 24040	-	$1.12^{+0.01}_{-0.02}$	$1.29^{+0.03}_{-0.02}$	$1.71^{+0.05}_{-0.05}$	$5.3^{+0.6}_{-0.4}$	$4.6^{+1.7}_{-1.3}$	$2.138^{+1.577}_{-0.908}$	-
HD 69809	-	$1.15^{+0.01}_{-0.01}$	$1.23^{+0.03}_{-0.01}$	$1.61^{+0.06}_{-0.04}$	$3.8^{+0.3}_{-0.3}$	$4.1^{+1.6}_{-1.1}$	$4.228^{+3.119}_{-1.795}$	-
HD 74698	0.039	$1.06^{+0.01}_{-0.01}$	$1.31^{+0.02}_{-0.02}$	$1.75^{+0.05}_{-0.05}$	$7.3^{+0.3}_{-0.3}$	$5.2^{+2.0}_{-1.4}$	$13.350^{+9.850}_{-5.668}$	-
HD 111398	-	$1.03^{+0.01}_{-0.01}$	$1.25^{+0.02}_{-0.02}$	$1.54^{+0.04}_{-0.05}$	$7.9^{+0.4}_{-0.4}$	$5.8^{+2.2}_{-1.6}$	$7.813^{+5.764}_{-3.317}$	-
HD 148577	-	$0.97^{+0.01}_{-0.01}$	$1.26^{+0.02}_{-0.02}$	$1.55^{+0.05}_{-0.04}$	$9.8^{+0.6}_{-0.6}$	$7.0^{+2.6}_{-2.0}$	$7.117^{+5.251}_{-3.022}$	-
HD 175425	-	$1.10^{+0.02}_{-0.02}$	$1.22^{+0.03}_{-0.03}$	$1.60^{+0.04}_{-0.05}$	$4.8^{+0.9}_{-0.9}$	$3.7^{+1.4}_{-1.0}$	$5.337^{+3.938}_{-2.266}$	-
HD 196050	0.028	$1.18^{+0.02}_{-0.01}$	$1.37^{+0.04}_{-0.02}$	$2.05^{+0.1}_{-0.04}$	$4.2^{+0.2}_{-0.4}$	$4.0^{+1.6}_{-1.1}$	$3.964^{+2.925}_{-1.683}$	-
HD 213575	-	$0.95^{+0.01}_{-0.01}$	$1.41^{+0.02}_{-0.02}$	$1.86^{+0.05}_{-0.05}$	$11.1^{+0.3}_{-0.3}$	$8.0^{+3.1}_{-2.2}$	$6.457^{+4.764}_{-2.741}$	-
Sun Today	-	1.00	1.00	1.00	-	-	-	-
HD 146233 (18 Sco)	-	$1.03^{+0.01}_{-0.01}$	$0.99^{+0.01}_{-0.01}$	$1.00^{+0.01}_{-0.04}$	$2.3^{+0.5}_{-0.6}$	$5.1^{+1.9}_{-1.4}$	$5.702^{+4.207}_{-2.421}$	-

with stars up to at least  $\sim 6$  Gyr with good precision, which encompass almost all of our sample. In other words, we consider the isochronal age as the most reliable at this stage. We, therefore, consider this star to be an excellent candidate to represent the Sun at the SG stage.

## 6. CONCLUSIONS

In this work, we analyzed 18 candidates for representing the Sun at two stages of its evolution: ZAMS and subgiant (SG). We utilized high-resolution spectra ( $R > 35000$ ) with high signal-to-noise ratio ( $SNR > 100$ ) to derive the atmospheric parameters of all candidates through the classical spectroscopic method, which uses equivalent widths of Fe I and Fe II lines and is based on the excitation and ionization equilibria. We calculated the evolutionary parameters of these stars by comparing stellar parameters with grid of isochrones. Additionally, we determined the kinematic parameters of each candidate and estimated their ages using three additional indicators: chromospheric emission in the H & K lines of Ca II, chromospheric emission in the  $H\alpha$  line and their rotation periods derived from their TESS light curves. Our methods allowed us perform a very detailed characterization of each of the sample candidates and select those that could represent the Sun at different stages of its life.

In particular, we should highlight the following candidates: HD 13531 (young Sun analog), HD 61033 (young Sun analog) and HD 148577 (SG). These stars are the most promising in the sample, with the first two stars being very active and practically indistinguishable from the Sun around its first 0.5 Gyr. Besides, these two candidates present a good agreement between the 4 different age indicators used in this work (isochronal, two chromospheric and rotational ages). With ages in the interval  $\approx 0.3 - 0.5$  Gyr, the young Sun candidate HD 13531 is very interesting, from an astrobiological perspective, because it could represent the Sun when life appeared on Earth (Archaeon Eon).

Therefore, this candidate is useful for a study of the habitability conditions in this type of stellar system, as well as priority target to search for exoplanets in future missions, when we will be able to detect Earth-sized planets in their habitable zones, for example, with the PLATO mission([H. Rauer et al. 2025](#)).

The star HD 148577, on the other hand, is an excellent candidate to represent the Sun at the end of the Main Sequence. Its isochronal age suggests that this star is close to the values expected for the turn-off point, in addition to having already undergone a considerable increase in its radius and luminosity values. From an astrobiological perspective, this candidate presents a unique opportunity for studying and monitoring environmental conditions as a possible host of old, evolved exoplanets.

Our pilot study demonstrated that the selection method used in this work is capable of identifying Sun-like stars at different evolutionary stages, broadening the understanding gained through the solar twins approach. Currently, we are expanding our sample through a new selection of candidates leveraging Gaia photometric data ([Gaia Collaboration et al. 2018](#)) as well as the more updated PARSEC evolutionary tracks ([A. Bressan et al. 2012](#)). These tools will allow us to perform a more comprehensive study and better understand the solar evolution and habitability in nearby planetary systems.

#### ACKNOWLEDGMENTS

E.-O.C.S. would also like to express my gratitude to Conselho Nacional de Desenvolvimento Científico e Tecnológico (CNPq) for financially supporting the project. Additionally, E.-O.C.S. would like to thank Fundação Coordenação de Aperfeiçoamento de Pessoal de Nível Superior (CAPES) for funding during my PhD (under grant number 88887.927885/2023-00), which enabled the development of this article. L.G. would like to thank the financial support from Fundação de Amparo à Pesquisa do Estado do Rio de Janeiro (FAPERJ) through the ARC grant number E-26/211.386/201. G.F.P.M. acknowledges financial support from CNPq/Brazil under grant 474972/2009-7. P.V.S.S. acknowledges CAPES/Brazil PhD scholarship under grant 88887.821758/2023-00. E.-O.C.S. and L.G. would like to thank Ignasi Ribas for his helpful suggestions regarding the final draft of the manuscript. We thank the staff of OPD/LNA for their considerable support during the many observation runs carried out during this project. The software IRAF ([D. Tody 1986, 1993](#)) was used throughout this work - IRAF is listed in the Astronomical Source Code Library as ascl:9911.002; The DOI is 10.5281/zenodo.5816743.

#### AUTHOR CONTRIBUTIONS

*Facilities:* MUSICOS(OPD/LNA)

*Software:* NumPy ([C. R. Harris et al. 2020](#)), Matplotlib ([J. D. Hunter 2007](#))

#### APPENDIX

#### REFERENCES

Amarsi, A. M., Liljegegren, S., & Nissen, P. E. 2022, A&A, 668, A68, doi: [10.1051/0004-6361/202244542](https://doi.org/10.1051/0004-6361/202244542)

Amarsi, A. M., Nissen, P. E., & Skúladóttir, Á. 2019, A&A, 630, A104, doi: [10.1051/0004-6361/201936265](https://doi.org/10.1051/0004-6361/201936265)

Arriagada, P. 2011, The Astrophysical Journal, 734, 70

Asplund, M., Grevesse, N., Sauval, A. J., & Scott, P. 2009, arXiv preprint arXiv:0909.0948

Barbato, D., Ségransan, D., Udry, S., et al. 2023, A&A, 674, A114, doi: [10.1051/0004-6361/202345874](https://doi.org/10.1051/0004-6361/202345874)

Barnes, S. A. 2007, ApJ, 669, 1167, doi: [10.1086/519295](https://doi.org/10.1086/519295)

Bazot, M., Creevey, O., Christensen-Dalsgaard, J., & Meléndez, J. 2018, Astronomy & Astrophysics, 619, A172

Bazot, M., Ireland, M., Huber, D., et al. 2011, Astronomy & Astrophysics, 526, L4

Berger, T. A., Huber, D., Van Saders, J. L., et al. 2020, The Astronomical Journal, 159, 280

Booth, R. A., & Owen, J. E. 2020, Monthly Notices of the Royal Astronomical Society, 493, 5079, doi: [10.1093/mnras/staa578](https://doi.org/10.1093/mnras/staa578)

**Table 10.** Consistency between the stellar parameters and the reference solar values at each stage. The columns in the table represent: star, the evolutionary stage for which the candidate was selected, effective temperature, logarithm of the surface gravity, metallicity, mass, radius, luminosity, chromospheric activity index ( $\log R'_{HK}$ ), isochrone age, ages derived from chromospheric activity indices ( $\log R'_{HK}$  and  $H\alpha$ ), rotational period, and kinematic properties. Ticks indicate that the parameters are consistent with the expected values within  $2\sigma$ . We use the “ $\approx$ ” symbol for values that were beyond but still close (less or equal to 0.02) to the  $2\sigma$  limits. For the effective temperatures ( $T_{eff}$ ), we adopted a threshold of up to 10K relative to the  $2\sigma$  limits. For ages, due to the large uncertainties in some measurements, the tick/X classification was based only on the central value and an approximate 1 Gyr interval.

Star	Candidate	$T_{eff}$	$\log g$	[Fe/H]	M	R	L	$\log R'_{HK}$	$Age_{iso}$	$Age_{HK}$	$Age_{H\alpha}$	$P_{rot}$	Kinematics
Sun ZAMS		5586	4.53	0.00	1.00	0.90	0.70	>-4.75	0.0	0.0	0.0	-	-
HD 13531	ZAMS	×	✓	✓	×	≈	≈	✓	✓	✓	✓	✓	✓
HD 21411	ZAMS	×	✓	×	×	×	×	✓	×	×	×	-	✓
HD 25918	ZAMS	≈	✓	≈	×	✓	✓	×	×	×	×	-	×
HD 55720	ZAMS	×	✓	×	×	✓	✓	×	×	×	×	-	×
HD 61033	ZAMS	≈	✓	✓	≈	≈	✓	✓	✓	✓	✓	✓	✓
HD 64114	ZAMS	✓	✓	✓	×	✓	✓	×	×	×	×	-	×
HD 182619	ZAMS	✓	✓	×	×	✓	✓	×	×	×	×	-	✓
HD 197210	ZAMS	✓	✓	✓	×	✓	≈	×	×	×	×	-	✓
Sun SG		5743	4.18	0.00	1.00	1.34	1.76	<-4.75	10.0	10.0	10.0	-	-
HD 15942	SG	×	×	×	×	×	×	✓	×	-	✓	-	✓
HD 19308	SG	×	×	×	×	×	×	✓	×	×	×	-	✓
HD 24040	SG	×	≈	×	×	✓	✓	✓	×	×	×	-	✓
HD 69809	SG	×	×	×	×	×	✓	✓	×	×	×	-	✓
HD 74698	SG	×	✓	×	×	✓	✓	✓	×	×	×	-	✓
HD 111398	SG	✓	×	×	≈	×	×	✓	×	×	×	-	✓
HD 148577	SG	✓	✓	✓	≈	×	×	✓	✓	×	×	-	✓
HD 175425	SG	×	✓	×	×	×	×	✓	×	×	×	-	✓
HD 196050	SG	×	✓	×	×	✓	×	✓	×	×	×	-	✓
HD 213575	SG	×	✓	×	×	×	✓	✓	✓	×	×	-	✓

Bouma, L. G., Palumbo, E. K., & Hillenbrand, L. A. 2023, ApJL, 947, L3, doi: [10.3847/2041-8213/acc589](https://doi.org/10.3847/2041-8213/acc589)

Bovy, J., Rix, H.-W., Green, G. M., Schlafly, E. F., & Finkbeiner, D. P. 2016, The Astrophysical Journal, 818, 130

Bressan, A., Marigo, P., Girardi, L., et al. 2012, Monthly Notices of the Royal Astronomical Society, 427, 127

Brown, E. L., Jeffers, S. V., Marsden, S. C., et al. 2022, MNRAS, 514, 4300, doi: [10.1093/mnras/stac1291](https://doi.org/10.1093/mnras/stac1291)

Carlos, M., Amarsi, A. M., Nissen, P. E., & Canocchi, G. 2025, A&A, 700, A127, doi: [10.1051/0004-6361/202554267](https://doi.org/10.1051/0004-6361/202554267)

Casagrande, L., Schönrich, R., Asplund, M., et al. 2011, Astronomy & Astrophysics, 530, A138

Castelli, F., & Kurucz, R. L. 2003, in IAU Symposium, Vol. 210, Modelling of Stellar Atmospheres, ed. N. Piskunov, W. W. Weiss, & D. F. Gray, A20, doi: [10.48550/arXiv.astro-ph/0405087](https://doi.org/10.48550/arXiv.astro-ph/0405087)

Cayrel de Strobel, G. 1996, The Astronomy and Astrophysics Review, 7, 243

Cayrel de Strobel, G., Knowles, N., Hernandez, G., & Bentolila, C. 1981, Astronomy and Astrophysics, vol. 94, no. 1, Jan. 1981, p. 1-11., 94, 1

Chen, Y., Bressan, A., Girardi, L., et al. 2015, Monthly Notices of the Royal Astronomical Society, 452, 1068

Choi, J., Dotter, A., Conroy, C., et al. 2016, The Astrophysical Journal, 823, 102

Choi, J., Dotter, A., Conroy, C., et al. 2016, ApJ, 823, 102, doi: [10.3847/0004-637X/823/2/102](https://doi.org/10.3847/0004-637X/823/2/102)

Connelly, J. N., Bizzarro, M., Krot, A. N., et al. 2012, Science, 338, 651, doi: [10.1126/science.1226919](https://doi.org/10.1126/science.1226919)

Cosentino, R., Lovis, C., Pepe, F., et al. 2012, in Ground-based and Airborne Instrumentation for Astronomy IV, ed. I. S. McLean, S. K. Ramsay, & H. Takami, Vol. 8446, International Society for Optics and Photonics (SPIE), 84461V, doi: [10.1117/12.925738](https://doi.org/10.1117/12.925738)

Coşkunoglu, B., Ak, S., Bilir, S., et al. 2011, Monthly Notices of the Royal Astronomical Society, 412, 1237

Dekker, H., D'Odorico, S., Kaufer, A., Delabre, B., & Kotzlowski, H. 2000, in Society of Photo-Optical Instrumentation Engineers (SPIE) Conference Series, Vol. 4008, Optical and IR Telescope Instrumentation and Detectors, ed. M. Iye & A. F. Moorwood, 534–545, doi: [10.1117/12.395512](https://doi.org/10.1117/12.395512)

Demarque, P., Woo, J.-H., Kim, Y.-C., & Sukyoung, K. Y. 2004, *The Astrophysical Journal Supplement Series*, 155, 667

Do Nascimento, J.-D., Takeda, Y., Meléndez, J., et al. 2013, *The Astrophysical Journal Letters*, 771, L31

Do Nascimento, J.-D., Barnes, S., Saar, S., et al. 2023, *The Astrophysical Journal*, 958, 57

Donati, J.-F. 2003, in *Solar Polarization*, Vol. 307, 41

Dorren, J. D., & Guinan, E. F. 1994, *The Astrophysical Journal*, 428, 805

Dos Santos, L. A., Meléndez, J., do Nascimento, J.-D., et al. 2016, *Astronomy & Astrophysics*, 592, A156

Dotter, A., Chaboyer, B., Jevremović, D., et al. 2008, *ApJS*, 178, 89, doi: [10.1086/589654](https://doi.org/10.1086/589654)

Dotter, A., Conroy, C., Cargile, P., & Asplund, M. 2017, *ApJ*, 840, 99, doi: [10.3847/1538-4357/aa6d10](https://doi.org/10.3847/1538-4357/aa6d10)

Dravins, D., Linde, P., Ayres, T., et al. 1993a, *Astrophysical Journal, Part 1 (ISSN 0004-637X)*, vol. 403, no. 1, p. 412-425., 403, 412

Dravins, D., Linde, P., Fredga, K., & Gahm, G. 1993b, *Astrophysical Journal, Part 1 (ISSN 0004-637X)*, vol. 403, no. 1, p. 396-411., 403, 396

Dravins, D., Lindegren, L., Nordlund, A., & Vandenberg, D. 1993c, *Astrophysical Journal, Part 1 (ISSN 0004-637X)*, vol. 403, no. 1, p. 385-395., 403, 385

Gaia Collaboration, Brown, A. G. A., Vallenari, A., et al. 2018, *A&A*, 616, A1, doi: [10.1051/0004-6361/201833051](https://doi.org/10.1051/0004-6361/201833051)

Gaidos, E. J. 1998, *Publications of the Astronomical Society of the Pacific*, 110, 1259

Galarza, J. Y., Lorenzo-Oliveira, D., Ferreira, T., et al. 2025, *The Astrophysical Journal*, 983, 70, doi: [10.3847/1538-4357/adb57b](https://doi.org/10.3847/1538-4357/adb57b)

Ghezzi, L. 2005, Bachelor's Thesis: SOL Project (Solar Origin and Life): The Search for the Sun Through Time, Observatório do Valongo/UFRJ. <http://hdl.handle.net/11422/20207>

Ghezzi, L., Cunha, K., Smith, V. V., & de la Reza, R. 2010, *The Astrophysical Journal*, 724, 154, doi: [10.1088/0004-637x/724/1/154](https://doi.org/10.1088/0004-637x/724/1/154)

Ghezzi, L., Martinez, C. F., Wilson, R. F., et al. 2021, *ApJ*, 920, 19, doi: [10.3847/1538-4357/ac14c3](https://doi.org/10.3847/1538-4357/ac14c3)

Ghezzi, L., Montet, B. T., & Johnson, J. A. 2018, *The Astrophysical Journal*, 860, 109

Gomes da Silva, J., Santos, N. C., Adibekyan, V., et al. 2021, *A&A*, 646, A77, doi: [10.1051/0004-6361/202039765](https://doi.org/10.1051/0004-6361/202039765)

Gonzalez, G. 2025, *Monthly Notices of the Royal Astronomical Society*, 541, 3043, doi: [10.1093/mnras/staf1149](https://doi.org/10.1093/mnras/staf1149)

Gray, R., Corbally, C., Garrison, R., et al. 2006, *The Astronomical Journal*, 132, 161

Gray, R. O., Corbally, C., Garrison, R., McFadden, M., & Robinson, P. 2003, *The Astronomical Journal*, 126, 2048

Green, G. M., Schlafly, E., Zucker, C., Speagle, J. S., & Finkbeiner, D. 2019, *The Astrophysical Journal*, 887, 93

Güdel, M., Guinan, E. F., & Skinner, S. L. 1997, *The Astrophysical Journal*, 483, 947

Gustafsson, B. 2025, *A&A Rv*, 33, 3, doi: [10.1007/s00159-025-00160-9](https://doi.org/10.1007/s00159-025-00160-9)

Habets, G., & Heintze, J. 1981, *Astronomy and Astrophysics Supplement Series*, vol. 46, Nov. 1981, p. 193-237., 46, 193

Hall, J. C., Henry, G. W., & Lockwood, G. W. 2007, *The Astronomical Journal*, 133, 2206

Hall, J. C., & Lockwood, G. 2000, *The Astrophysical Journal*, 545, L43

Hardorp, J. 1978, *Astronomy and Astrophysics*, vol. 63, no. 3, Feb. 1978, p. 383-390., 63, 383

Harris, C. R., Millman, K. J., van der Walt, S. J., et al. 2020, *Nature*, 585, 357, doi: [10.1038/s41586-020-2649-2](https://doi.org/10.1038/s41586-020-2649-2)

Heiter, U., Jofré, P., Gustafsson, B., et al. 2015, *Astronomy & Astrophysics*, 582, A49

Henry, T. J., Soderblom, D. R., Donahue, R. A., & Baliunas, S. L. 1996, *AJ*, 111, 439, doi: [10.1086/117796](https://doi.org/10.1086/117796)

Hinkel, N. R., Young, P. A., Pagano, M. D., et al. 2016, *ApJS*, 226, 4, doi: [10.3847/0067-0049/226/1/4](https://doi.org/10.3847/0067-0049/226/1/4)

Hinkle, K., Wallace, L., Valenti, J., & Harmer, D. 2000, *Visible and Near Infrared Atlas of the Arcturus Spectrum 3727-9300 A*

Høg, E., Fabricius, C., Makarov, V. V., et al. 2000, *A&A*, 355, L27

Huber, D., Zinn, J., Bojsen-Hansen, M., et al. 2017, *The Astrophysical Journal*, 844, 102

Hunter, J. D. 2007, *Computing in Science & Engineering*, 9, 90, doi: [10.1109/MCSE.2007.55](https://doi.org/10.1109/MCSE.2007.55)

Isaacson, H., & Fischer, D. 2010, *The Astrophysical Journal*, 725, 875, doi: [10.1088/0004-637x/725/1/875](https://doi.org/10.1088/0004-637x/725/1/875)

Jenkins, J., Jones, H., Pavlenko, Y., et al. 2008, *Astronomy & Astrophysics*, 485, 571

Jenkins, J. S., Murgas, F., Rojo, P., et al. 2011, *Astronomy & Astrophysics*, 531, A8

Jurkevich, I. 1971, *Astrophysics and Space Science*, 13, 154

Kaufer, A., Wolf, B., Andersen, J., & Pasquini, L. 1997, *The Messenger*, vol. 89, p. 1-4, 89, 1

King, J. R., Boesgaard, A. M., & Schuler, S. C. 2005, *The Astronomical Journal*, 130, 2318

Kiselman, D. 2001, *New Astronomy Reviews*, 45, 559, doi: [https://doi.org/10.1016/S1387-6473\(01\)00127-0](https://doi.org/10.1016/S1387-6473(01)00127-0)

Krissansen-Totton, J., Wogan, N., Thompson, M., & Fortney, J. J. 2024, *Nature communications*, 15, 8374

Lehmann, C., Murphy, M. T., Liu, F., Flynn, C., & Berke, D. A. 2022, *Monthly Notices of the Royal Astronomical Society*, 512, 11

Leitch, E. M., & Vasisht, G. 1998, *New Astronomy*, 3, 51

Lépine, J., Mishurov, Y. N., & Dedikov, S. Y. 2001, *The Astrophysical Journal*, 546, 234

Lightkurve Collaboration, Cardoso, J. V. d. M., Hedges, C., et al. 2018,

Lind, K., & Amarsi, A. M. 2024, *ARA&A*, 62, 475, doi: [10.1146/annurev-astro-052722-103557](https://doi.org/10.1146/annurev-astro-052722-103557)

Lodders, K. 2003, *The Astrophysical Journal*, 591, 1220, doi: [10.1086/375492](https://doi.org/10.1086/375492)

Lorenzo-Oliveira, D., de Mello, G. P., & Schiavon, R. P. 2016, *Astronomy & Astrophysics*, 594, L3

Lorenzo-Oliveira, D., Freitas, F. C., Meléndez, J., et al. 2018, *Astronomy & Astrophysics*, 619, A73

Lorenzo-Oliveira, D., Freitas, F. C., Meléndez, J., et al. 2018, *A&A*, 619, A73, doi: [10.1051/0004-6361/201629294](https://doi.org/10.1051/0004-6361/201629294)

Lyra, W., & Porto de Mello, G. F. 2005, *A&A*, 431, 329, doi: [10.1051/0004-6361:20040249](https://doi.org/10.1051/0004-6361:20040249)

Mamajek, E. E., & Hillenbrand, L. A. 2008, *The Astrophysical Journal*, 687, 1264, doi: [10.1086/591785](https://doi.org/10.1086/591785)

Mamajek, E. E., & Hillenbrand, L. A. 2008, *ApJ*, 687, 1264, doi: [10.1086/591785](https://doi.org/10.1086/591785)

MAST. 2021, TESS Light Curves – All Sectors, Mikulski Archive for Space Telescopes, doi: [10.17909/t9-nmc8-f686](https://doi.org/10.17909/t9-nmc8-f686)

Mayor, M., Pepe, F., Queloz, D., et al. 2003, *The Messenger*, 114, 20

Meléndez, J., Asplund, M., Gustafsson, B., & Yong, D. 2009, *The Astrophysical Journal*, 704, L66, doi: [10.1088/0004-637x/704/1/l66](https://doi.org/10.1088/0004-637x/704/1/l66)

Meléndez, J., Ramirez, I., Karakas, A. I., et al. 2014, *The Astrophysical Journal*, 791, 14

Middelkoop, F. 1982, *Astronomy and Astrophysics*, 107, 31

Nieva, M.-F., & Przybilla, N. 2012, *Astronomy & Astrophysics*, 539, A143

Önehag, A., Korn, A., Gustafsson, B., Stempels, E., & VandenBerg, D. A. 2011, *Astronomy & Astrophysics*, 528, A85

Pace, G., & Pasquini, L. 2004, *Astronomy & Astrophysics*, 426, 1021

Pasquini, L., Liu, Q., & Pallavicini, R. 1994, *Astronomy and Astrophysics* (ISSN 0004-6361), vol. 287, no. 1, p. 191-205, 287, 191

Pasquini, L., & Pallavicini, R. 1991, *A&A*, 251, 199

Perryman, M. A., Lindegren, L., Kovalevsky, J., et al. 1997, *Astronomy and Astrophysics*, Vol. 323, p. L49-L52, 323, L49

Porto de Mello, G., & da Silva, L. 1997, *The Astrophysical Journal*, 482, L89

Porto de Mello, G., Da Silva, R., Da Silva, L., & De Nader, R. 2014, *Astronomy & Astrophysics*, 563, A52

Porto de Mello, G., Fernandez del Peloso, E., & Ghezzi, L. 2006, *Astrobiology*, 6, 308, doi: [10.1089/ast.2006.6.308](https://doi.org/10.1089/ast.2006.6.308)

Porto de Mello, G. F., Lépine, J. R., & da Silva Dias, W. 2009, in *Astronomical Society of the Pacific Conference Series*, Vol. 420, *Bioastronomy 2007: Molecules, Microbes and Extraterrestrial Life*, ed. K. J. Meech, J. V. Keane, M. J. Mumma, J. L. Siefert, & D. J. Werthimer, 349

Pownall, M. W., Gerland, B., & Sutherland, J. D. 2009, *Nature*, 459, 239

Prša, A., Harmanec, P., Torres, G., et al. 2016, *The Astronomical Journal*, 152, 41

Radick, R. R., Lockwood, G. W., Henry, G. W., Hall, J. C., & Pevtsov, A. A. 2018, *The Astrophysical Journal*, 855, 75

Ramírez, I., Fish, J., Lambert, D. L., & Prieto, C. A. 2012, *The Astrophysical Journal*, 756, 46

Ramírez, I., Meléndez, J., Bean, J., et al. 2014, *Astronomy & Astrophysics*, 572, A48

Rampalli, R., Ness, M. K., Edwards, G. H., Newton, E. R., & Bedell, M. 2024, *ApJ*, 965, 176, doi: [10.3847/1538-4357/ad303e](https://doi.org/10.3847/1538-4357/ad303e)

Rauer, H., Aerts, C., Cabrera, J., et al. 2025, *Experimental Astronomy*, 59, 26, doi: [10.1007/s10686-025-09985-9](https://doi.org/10.1007/s10686-025-09985-9)

Reinhold, T., & Hekker, S. 2020, *Astronomy & Astrophysics*, 635, A43

Reinhold, T., Shapiro, A. I., Solanki, S. K., et al. 2020, *Science*, 368, 518, doi: [10.1126/science.aay3821](https://doi.org/10.1126/science.aay3821)

Ribas, I., Guinan, E. F., Güdel, M., & Audard, M. 2005, *The Astrophysical Journal*, 622, 680

Ribas, I., De Mello, G. P., Ferreira, L., et al. 2010, *The Astrophysical Journal*, 714, 384

Ricker, G. R., Latham, D. W., Vanderspek, R. K., et al. 2010, in *American Astronomical Society Meeting Abstracts*, Vol. 215, *American Astronomical Society Meeting Abstracts #215*, 450.06

Rocha-Pinto, H. J., & Maciel, W. J. 1996, *Monthly Notices of the Royal Astronomical Society*, 279, 447, doi: [10.1093/mnras/279.2.447](https://doi.org/10.1093/mnras/279.2.447)

Rutten, R. 1984, *Astronomy and Astrophysics* (ISSN 0004-6361), vol. 130, no. 2, Jan. 1984, p. 353-360., 130, 353

Sackmann, I., Boothroyd, A. I., Kraemer, K. E., et al. 1993, *Astrophysical Journal* v. 418, p. 457, 418, 457

Samus', N. N., Kazarovets, E. V., Durlevich, O. V., Kireeva, N. N., & Pastukhova, E. N. 2017, *Astronomy Reports*, 61, 80, doi: [10.1134/S1063772917010085](https://doi.org/10.1134/S1063772917010085)

Schaller, G., Schaefer, D., Meynet, G., & Maeder, A. 1992, *Astronomy and Astrophysics Supplement Series*, 96, 269

Sneden, C. A. 1973, Ph.D. thesis, University of Texas at Austin

Soubiran, C., & Triaud, A. 2004, *Astronomy & Astrophysics*, 418, 1089

Sousa, S., Santos, N., Adibekyan, V., Delgado-Mena, E., & Israelian, G. 2015, *Astronomy & Astrophysics*, 577, A67

Sousa, S., Santos, N. C., Israelian, G., Mayor, M., & Monteiro, M. 2007, *Astronomy & Astrophysics*, 469, 783

Souza dos Santos, P. V., Porto de Mello, G. F., Costa-Bhering, E., et al. 2024, *Monthly Notices of the Royal Astronomical Society*, 532, 563

Stellingwerf, R. F. 1978, *Astrophysical Journal*, Part 1, vol. 224, Sept. 15, 1978, p. 953-960., 224, 953

Takeda, Y., Kawanomoto, S., Honda, S., Ando, H., & Sakurai, T. 2007, *A&A*, 468, 663, doi: [10.1051/0004-6361:20077220](https://doi.org/10.1051/0004-6361:20077220)

Tody, D. 1986, in *Society of Photo-Optical Instrumentation Engineers (SPIE) Conference Series*, Vol. 627, *Instrumentation in astronomy VI*, ed. D. L. Crawford, 733, doi: [10.1117/12.968154](https://doi.org/10.1117/12.968154)

Tody, D. 1993, in *Astronomical Society of the Pacific Conference Series*, Vol. 52, *Astronomical Data Analysis Software and Systems II*, ed. R. J. Hanisch, R. J. V. Brissenden, & J. Barnes, 173

Turnbull, M. C., & Tarter, J. C. 2003, *The Astrophysical Journal Supplement Series*, 145, 181, doi: [10.1086/345779](https://doi.org/10.1086/345779)

VanderPlas, J. T. 2018, *The Astrophysical Journal Supplement Series*, 236, 16

Vaughan, A. H., Preston, G. W., & Wilson, O. C. 1978, *Publications of the Astronomical Society of the Pacific*, 90, 267, doi: [10.1086/130324](https://doi.org/10.1086/130324)

Vogt, S. S., Allen, S. L., Bigelow, B. C., et al. 1994, in *Instrumentation in Astronomy VIII*, Vol. 2198, SPIE, 362-375

Walker, G. A. H., Croll, B., Kuschnig, R., et al. 2007, *ApJ*, 659, 1611, doi: [10.1086/511851](https://doi.org/10.1086/511851)

Wright, J. T., Marcy, G. W., Butler, R. P., & Vogt, S. S. 2004, *The Astrophysical Journal Supplement Series*, 152, 261

Yana Galarza, J., López-Valdivia, R., Lorenzo-Oliveira, D., et al. 2021, *Monthly Notices of the Royal Astronomical Society*, 504, 1873, doi: [10.1093/mnras/stab987](https://doi.org/10.1093/mnras/stab987)